Supplementary Materials

Dror et al., "Structural Basis for Nucleotide Exchange in Heterotrimeric G Proteins"

Materials and Methods

Molecular Dynamics Simulations

In this work, we describe 66 simulations of heterotrimeric G proteins totaling 635 µs (Table S1). All simulations were performed on Anton (*1*, *2*), a special-purpose computer designed to accelerate standard molecular dynamics simulations by orders of magnitude. All simulations included the full heterotrimer (i.e., the α and βγ subunits), except for the three simulations of the GTP-bound condition, which include only the α subunit because the α and βγ subunits dissociate under this condition. In all simulations without bound GTP, the G protein α and βγ subunits remained associated, in accord with experimental observations (*3*).

Initial coordinates and system setup

We prepared all-atom molecular dynamics simulations of GDP-bound $G\alpha_{ti}\beta_1\gamma_1$ heterotrimer (G_t) and GDP-bound $G\alpha_{i1}\beta_1\gamma_2$ heterotrimer (G_i) using their respective crystal structures (for G_t, PDB entry 1GOT [*4*]; for G_i, PDB entry 1GP2 [*5*]). In the G_t crystal structure, α subunit residues 216–294 of G_t were substituted with residues 220–298 from G_{i1} to improve protein expression (*6*); we retained these substitutions in our G_t simulations.

We prepared simulations of G_t heterotrimer in unliganded, GMP-bound, or pyrophosphate-bound states by removing part or all the GDP present in the crystal structure (for pyrophosphate, we added a proton to obtain $HP_2O_7^{3-}$). We prepared foscarnet-bound G_t heterotrimer by retaining the β-phosphate and converting the bridging oxygen to a carboxyl group. We also prepared a variant of G_t heterotrimer with its helical domain removed ($G_t\Delta HD$); for these simulations, α subunit residues 58–174 were removed and the resulting termini capped with N-terminal acetyl and C-terminal methylamide groups.

G proteins are typically attached to membranes, but are also functional in solution. Some of our G_t simulations included a membrane (see Table S1), for which we used an equilibrated palmitoyl-oleoyl-phosphatidylcholine (POPC)/palmitoyl-oleoyl-phosphatidylserine (POPS) bilayer; the G protein–facing leaflet was 70% POPC and 30% POPS, while the other leaflet was 100% POPC. In these simulations, we modeled in the α-subunit *N*-myristoyl Gly2 and γ-subunit *S*-farnesyl Cys71 groups. Most of our simulations omitted the membrane for computational efficiency reasons. These simulations without the membrane also omitted the lipid modifications. These differences do not appear to affect the features discussed in this work (Figure S17).

We prepared simulations of nucleotide-free $G\alpha_s\beta_1\gamma_2$ heterotrimer (G_s) in complex with agonist-bound β₂-adrenergic receptor (β₂AR) using the crystal structure of nucleotide-free G_s in complex with a camelid nanobody and an agonist-bound β₂AR–T4L fusion protein (PDB entry 3SN6) (*7*). As in other structures of β₂AR, intracellular loop 3 is unresolved in this structure; we modeled this loop in an extended conformation away from the resolved structure. We also modeled in missing residues 176–178 in extracellular loop 2. We removed the co-crystallized T4L and nanobody and added a palmitoyl group to β₂AR Cys341. Because they contain β₂AR, all of these simulations included a membrane (with the lipid composition described above), and we also included the native G_s lipid-modifications α-subunit *N*-palmitoyl Gly2, *S*-palmitoyl Cys3, and γ-subunit *S*-geranylgeranyl Cys71. Simulation 65 represented the short isoform of G_s, which

2

is the crystallized construct. Simulations 22–24 represented the long isoform, which has an additional loop between helices α1 and αA; we modeled in this additional loop. We did not observe any substantive differences in behavior between the two isoforms. Finally, we prepared simulations of GTP/Mg^{2+}-bound Gα$_{ti}$ monomer (Gα$_t$) using the crystal structure of the chimeric G$_t$ α subunit (see above) in a GDP/AlF$_4$/Mg^{2+}-bound state in complex with the RGS domain from RGS9 and the PDE gamma subunit (PDB entry 1FQJ) (*8*). AlF$_4$ is widely used as a reagent to convert GDP-bound G proteins to their active state without the need for nucleotide exchange; indeed, the α subunit in this structure and the structure of GTPγS/Mg^{2+}-bound wild-type Gα$_t$ alone (PDB entry 1TND) (*9*) are almost identical (excluding the C-termini, Cα RMSD < 0.5 Å). We chose to use the structure with co-crystallized RGS and PDE domains because it features the same chimeric α subunit as the structure of heterotrimeric G$_i$. Lastly, we converted AlF$_4$ into the γ phosphate of GTP, taking care to maintain the proper octahedral Mg^{2+}-coordination geometry.

We modeled the crystallographically unresolved N- and C-termini in various ways in our simulations and found that these differences do not affect the features described in this work (Figure S17). In the first group of simulations (7–12, 16–18, 31–32, and 59–64), the resolved crystal structures were simply capped with N-terminal acetyl and C-terminal methylamide groups on each chain. In a second group, which corresponded to all simulations with a membrane (1–3, with G$_t$; 22–24 and 65, with G$_s$), we modeled the native G proteins: the α and γ subunit N-termini were extended to residue 2 (the initiator methionine is typically absent in these proteins), the α subunit C-terminus was modeled fully (to α$_t$ Phe350; α$_s$ is already resolved through Leu394), the β subunit N-terminus was capped with an acetyl, the γ subunit C-terminus was fully extended (to γ$_t$ residue 71 or γ$_2$ residue 68) and carboxymethylated, and the native G protein lipid modifications were included. Simulations 22–24 and 65 also included a β$_2$AR comprising residues 29–351 and capped with acetyl and *N*-methylamide groups. A third and final group of simulations (4–6, 13–15, 19–21, 25–26, 33–58, and 66, all with G$_t$, and 27–30, with G$_i$) omitted the membrane but included most of the crystallographically unresolved N- and C-terminal residues. For these simulations, the α and γ subunit N-termini were modeled to

residue 2, the α subunit C-terminus was modeled fully (to α_t Phe350 or α_i Phe354), and the γ subunit C-terminus was modeled to residue 68. N-terminal acetyl caps were added to the α and β subunits in all simulations and no C-terminal acetyl caps were added to any of the subunits. In the G_i simulations (simulations 27–30), an N-terminal cap was added to the γ subunit and C-terminal residue 68 was carboxymethylated but not farnesylated. In the G_t simulations (simulations 4–6, 13–15, 19–21, 25–26, 33–58, and 66), the N-terminus was uncapped and the C terminus was left as a naked carboxyl, to reflect the crystallized construct as prepared by proteolysis.

All systems were solvated with roughly 0.15 M KCl in explicitly represented water (we used K^+ cations rather than Na^+ cations to reflect the intracellular environment where G proteins are found). A few ions were added or removed to neutralize each system prior to simulation. Glu122 and Asp130 of β_2AR were protonated (neutral) in simulations; all other acidic residues of β_2AR and G proteins were deprotonated (charged). All histidines were singly protonated (neutral).

Final system compositions were as follows. Heterotrimeric G proteins in the absence of a membrane ranged from around 145,000 atoms in a 115 × 115 × 115 Å box, including roughly 44,000 water molecules, 147 potassium ions, and 123 chloride ions, to 172,000 atoms in a 122 × 122 × 122 Å box, including roughly 53,000 water molecules, 174 potassium ions, and 148 chloride ions. G proteins with membrane comprised around 234,000 atoms in a 122 × 122 × 150 Å box, including roughly 53,000 water molecules, 143 potassium ions, and 41 chloride ions. The $\beta_2AR–G_s$ complex comprised around 232,000 atoms in a 126 × 126 × 143 Å box, including roughly 52,000 water molecules, 140 potassium ions, and 69 chloride ions. All systems were simulated using periodic boundary conditions.

Force field parameters

We used the CHARMM27 parameter set for protein molecules and salt ions and the CHARMM TIP3P model for water (*10*); protein parameters incorporated CMAP terms (*11*) and modified Asp, Glu, and Arg side-chain partial charges (*12*). We used a modified CHARMM lipid force field (*13*). Force field parameters for palmitoyl-cysteine and BI-167107 (the β_2AR agonist) were designed previously (*14, 15*). The ParamChem server (versions 0.9.1, 0.9.6; ref. *16*) was used to obtain parameters for the lipid-modified amino acids (*N*-palmitoylglycine, *N*-myristoylglycine, *S*-farnesyl carboxymethylcysteine, and *S*-geranylgeranyl carboxymethylcysteine). ParamChem was also used to generate nucleotide parameters, but these parameters directly matched CGenFF templates (version 2b6; ref. *16*) except for miniscule charge discrepancies (under 0.02 e⁻). For simulation 26, the charges for foscarnet were refitted using a quantum chemical method. Full parameter sets are available upon request.

Simulation protocol

Simulations were performed as described previously (*17*). Simulations without membranes consisted of a 50-ns equilibration run followed by a longer production run (except simulations 7 and 10–12, which had 20-ns equilibrations). Simulations containing a membrane were equilibrated for 500 ns to allow additional time for lipid diffusion. Systems were equilibrated in the NPT ensemble (310 K, 1 bar, Martyna-Tuckerman-Klein Nosé-Hoover chain coupling scheme; *18*) using a multigrator (*19*), with initial velocities sampled from the Boltzmann distribution. 5 kcal mol^{-1} Å^{-2} harmonic position restraints applied to most non-hydrogen atoms of the proteins and ligands and tapered off linearly over the equilibration; these restraints were not included for non-crystallographic atoms that were modeled in, allowing them to relax. Production simulations used the same integrator, pressure and temperature, and were initiated from the final snapshot of the corresponding equilibration simulation, with velocities often resampled from the Boltzmann distribution at 310 K.

All bond lengths to hydrogen atoms were constrained using M-SHAKE (*20*). An r-RESPA integrator (*21*) was used with a time step of 2.33 fs, and long-range electrostatics were computed every 6.99 fs. Long-range electrostatics were computed using the *k*-space Gaussian split Ewald method (*k*-GSE; *22*) with a 64 × 64 × 64 grid. The *k*-GSE parameters σ and σ_s, as well as the cut-off parameter Rcut for the van der Waals and short-range electrostatic interactions, were chosen to ensure low force errors and were as follows: for β_2AR–G_s simulations, Rcut = 14.87 Å, σ = 3.17 Å, and σ_s = 2.22 Å; for membrane-associated G_t simulations without receptor, Rcut = 13.19 Å, σ = 3.07 Å, and σ_s = 2.04 Å; for simulations of G proteins without membrane, various parameters within the ranges Rcut = 11.7–13.6 Å, σ = 2.7–2.8 Å, and σ_s = 1.5–1.7 Å. Root-mean-squared force errors were no more than 0.0025 kcal mol^{-1} Å^{-1} for the initial configuration of each system.

Opening-limiting restraints

To investigate the role of interdomain separation in nucleotide release, we ran several simulations in which the distance between the Ras and helical domains was restrained from exceeding a certain distance. In particular, the Cα atoms of α subunit residues 134 and 272 were subject to a flat-bottomed harmonic restraint (i.e., a restraint whose energy is zero up to some cut-off value and then grows with the square of the difference between the distance and that cut-off value). To prevent opening entirely, the restraint was applied at distances exceeding 16 Å with spring constant 1 kcal mol^{-1} Å^{-2}. To allow some opening, similar restraints were applied except that the spring constant was 2.5 kcal mol^{-1} Å^{-2} and the restraints began at either 30 Å (simulation 62) or 40 Å (simulations 63 and 64).

Temperature-accelerated molecular dynamics

Temperature-accelerated molecular dynamics (TAMD) (*23*) is a method for enhancing sampling along a chosen set of collective variables (CVs) (e.g., the coordinates of the centroid of a group

6

of atoms). The acceleration is achieved by tethering a CV to a fictitious particle undergoing Brownian motion at a higher temperature. With a proper choice of parameters, the sampling of the chosen CV is accelerated such that the fictitious particles still obey Boltzmann statistics at the higher, fictitious temperature, T_s, while the non-accelerated orthogonal degrees of freedom of the real system remain properly distributed at the real temperature. In the TAMD simulations, the center of mass of the non-hydrogen atoms of the GDP was accelerated. For these simulations, the spring constant tethering the CV to the fictitious particle was 2000 kcal mol^{-1} Å^{-2} and the friction coefficient for the fictitious particle was 100 ps kcal mol^{-1} Å^{-2}, giving a time constant of 0.05 ps. The fictitious temperature T_s was chosen such that $k_B T_s$ was 2.0 kcal mol^{-1}.

In certain TAMD simulations (simulations 37, 38), the α carbons of six residues in the Gα$_t$ β sheet far from the bound nucleotide—residues 30, 186, 191, 216, 260, and 316—were restrained (using 5 kcal mol^{-1} Å^{-2} harmonic position restraints) to ensure that acceleration of the nucleotide did not lead to overall motion of the protein, which could in principle dampen the effect of the TAMD. In practice, this did not appear to be a substantive issue, most likely because the time constant of TAMD was much more rapid than the protein diffusion timescale (nanoseconds).

Receptor-mimicking restraints

The β$_2$AR–G$_s$ crystal structure (PDB entry 3SN6) provides the only atomic-resolution information about the full G protein conformation that interacts with a receptor. To mimic the effect of a receptor on a G protein, 5 kcal mol^{-1} Å^{-2} harmonic position restraints were applied to target (i.e., push) certain atoms in Gα$_t$ to the positions of corresponding atoms in the β$_2$AR–G$_s$ crystal structure. We started with the Gα$_s$ residues within 5 Å of β$_2$AR: in simulations 39–41, the α carbons of α$_t$ residues 23, 27, 28, 30, 190, 192, 300, 301, 304, 305, 308, 314, 317, 332, 335–337, 339–341, 343, 344, and 347–350 were targeted to the positions of the corresponding α$_s$

residues 34, 38, 39, 41, 217, 219, 342, 343, 346, 347, 350, 358, 361, 376, 379–381, 383–385, 387, 388, and 391–394. In simulations 42–44 and 56–58, we targeted residues within 4 Å of the receptor; i.e., the restraints were applied similarly except that α_t residues 23, 192, 300, 308, and 317 were omitted (also, the F332 ζ carbon was added, in order to overcome a tendency of the F332 side chain to get stuck even as its backbone was repositioned). As a control, in simulations 45–47, we targeted residues within 4 Å of the receptor *excluding* the α5 helix; thus, only the α carbons from α_t residues 27, 28, 30, 190, 301, 304, 305, and 314 were restrained. Simulations 48–54 are older simulations included here for completeness. (Conceptually, simulations 49–54 are similar to 56–58; simulation 48 is also similar, but without TAMD.) In simulations 48–54, restraints were applied in two phases. During equilibration, the α carbons in residues 30–33, 181–186, 191–195, 216–219, 260–263, 316–318, and 340–350 (corresponding to the β sheet and the end of α5) were restrained; then during production, only the α carbons from α_t residues 30, 186, 191, 216, 260, 316, and 340–350 were restrained, representing α5 and residues in the β sheet far from the bound nucleotide.

Analysis protocols

Simulation snapshots were saved every 180 ps. Time traces were computed from these snapshots. For clarity, traces are shown in figures as moving averages, where each value represents the mean of data from about 1/100th of the full time axis of the figure (i.e., over a 100–500 ns window). In some figures, unsmoothed traces are also shown using lighter colors (except where noted otherwise, these unsmoothed traces have been down-sampled).

VMD (Visual Molecular Dynamics; *24*) was used to visualize trajectories and produce molecular renderings. To facilitate comparisons with crystal structures where these features were unresolved or absent, we omitted from renderings of β₂AR–Gₛ simulation snapshots two loops that were modeled in before simulation: the third intracellular loop in β₂AR (residues 240–264) and an interdomain connector loop present in the long isoform of Gαₛ (residues 60–87).

Foscarnet- and pyrophosphate-bound simulations

Foscarnet and pyrophosphate interact most tightly with the P-loop and α1 helix of the Ras domain in simulation. Because these ligands lack interactions with the β6–α5 loop, they appear much less stably bound in simulation than GDP; in some of the simulations, foscarnet and pyrophosphate dissociated from the P-loop. As might be expected, the absence of the guanosine moiety leads to increased mobility in the β6–α5 loop and the α5 helix. In one of the foscarnet-bound simulations, displacement of the β6–α5 loop from its crystallographic (GDP-bound) position is accompanied by a concurrent displacement of α1 and the P-loop, followed by dissociation of foscarnet from the P-loop. This suggests that conformational changes in the α5 helix and the β6–α5 loop may destabilize the P-loop, but we do not have enough data to draw conclusions about this with confidence.

DEER Experiments

In a previous study, Van Eps *et al.* used site-directed spin labeling in combination with X-band DEER distance measurements to examine separation between the Ras and helical domains of G_i upon receptor binding (*25*). For GDP-bound G_i heterotrimer in the absence of the receptor, they observed small peaks at long distances in the interdomain distance distributions. Interpreting the significance of the peaks observed in the Van Eps *et al.* study is challenging for several reasons, each of which we sought to address in the present study.

First, due to the typically short transverse relaxation times of spin labels in aqueous buffers, the dipolar evolution time (t_{max}) employed by Van Eps *et al.* was not long enough to be fully confident about the shape and widths of the peaks at long distances. To increase confidence in the measured distance distributions in the long-distance range (30–50 Å), we performed DEER distance measurements on doubly spin-labeled G proteins in deuterated buffer and with deuterated glycerol as a cryoprotectant to decrease proton spin diffusions and to increase t_{max}.

With these modifications in the experimental setup, we obtained high quality data with t_{max}

values up to 5.2 µs.

Second, the signal-to-noise ratio in the previous study was relatively low. We achieved higher

signal-to-noise ratios by collecting data at higher microwave frequencies (Q-band, 34 GHz) and

suppressing nuclear modulation artifacts (*26–28*).

Third, the minimal-cysteine G_i construct used in the previous study included a 6x histidine tag

between residues Met119 and Thr120 of the helical domain. To avoid any possible influence of

such an insertion on the dynamics of the helical domain, we used an alternative minimal-cysteine

G_i construct with no inserted tag. (We moved the 6x histidine tag to the amino terminus of the α

subunit and followed it by a rhinovirus 3C protease site, which allowed us to remove the tag after

purification and before DEER experiments.)

Fourth, we performed a similar experiment on G_s to verify that similar long-distance peaks are

observed in another G protein.

Construction, expression, and purification of proteins for DEER measurements

Human Gα$_i$ and Gα$_s$ subunits with an amino-terminal 6x histidine tag followed by a rhinovirus

3C protease side were expressed in Rosetta 2 (DE3) cells (EMD Millipore) using pET28a. To

allow for site-directed spin labeling of the Gα subunits, minimal cysteine derivatives were

generated by removal of reactive cysteines. The Gα$_i$Δ6 construct includes C3S, C66A, C214S,

C305S, C325A, and C351I, as published previously (*29*). For Gα$_s$, we developed a minimal

cysteine construct based on cysteine accessibility studies using fluorescent labeling and mass

spectrometry (data not shown). In the mutant Gα$_s$Δ5, five cysteine residues were substituted

(C3S, C200T, C237S, C359I, and C379V) to generate a protein free of background labeling. For

DEER studies, residues R90 and E238 in Gαi Δ6 (*25*) and the corresponding residues N112 and

N261 in Gα$_s$Δ5 were simultaneously mutated to cysteine to create Gα$_i$Δ6-R90C/E238C and Gα$_s$Δ5-N112C/N261C.

Rosetta 2 (DE3) cells transformed with the mutant plasmids were grown in Terrific Broth to OD600 of 0.6, and protein expression was induced by addition of 0.5 mM IPTG. After 15 h of incubation at room temperature, cells were harvested and resuspended in lysis buffer (50 mM HEPES pH 7.5, 100 mM sodium chloride, 2 mM magnesium chloride, 50 µM GDP, 5 mM beta-mercaptoethanol, 5 mM imidazole, and protease inhibitors). Cells were disrupted by three passes at 15,000 psi using a high-pressure homogenizer. Intact cells and cell debris were subsequently removed by centrifugation and the supernatant was incubated with Ni-NTA resin for 1.5 h at 4 °C. The Ni-NTA resin was washed multiple times with lysis buffer in batch and then loaded into a wide-bore glass column, and protein was eluted with lysis buffer containing 200 mM imidazole. The eluted protein was dialyzed overnight in dialysis buffer (20 mM HEPES pH 7.5, 100 mM sodium chloride, 1 mM magnesium chloride, 50 µM GDP, 5 mM beta-mercaptoethanol, and 5 mM imidazole). The amino terminal histidine tag was cleaved by adding 1:1000 w/w 3C protease into the dialysis bag. Uncleaved protein, cleaved histidine tag, and 3C protease were subsequently removed by incubation with Ni-NTA resin for 45 min at 4 °C. The resin was loaded into a wide-bore glass column and the flow-through containing the Gα subunit was collected.

The Gβγ heterodimer for DEER measurements was expressed and purified similarly to the G protein heterotrimer (see above), with omission of GDP and magnesium chloride. Before freezing the protein, reducing agent was removed and buffer exchanged into deuterated buffer (20 mM HEPES pH 7.5 and 100 mM sodium chloride) by extensive washing in a 30 kDa MWCO centrifugal ultrafiltration device (EMD Millipore). 20% deuterated glycerol (Cambridge Isotopes) was added to concentrated protein, followed by aliquoting and flash freezing of the protein in liquid nitrogen.

The Gβγ heterodimer for DEER measurements was expressed in *Hi5* cells using a baculovirus generated by the BestBac (Expression systems) method. We used one virus containing the genes for Gβ and Gγ subunits. The sequence for the Gβ subunit contains an amino terminal 6x histidine tag followed by a rhinovirus 3C protease sequence, allowing us to cleave off the histidine tag after purificiation. *Hi5* cells were infected at a density of 3.0×10^6 cells/ml and incubated at 27 °C for 48 h. After centrifugation, cells were resuspended in lysis buffer (10 mM Tris, pH 7.5, 5 mM beta-mercaptoethanol, and protease inhibitors). The membrane fraction was collected by centrifugation and solubilized by a dounce homogenizer with a buffer comprised of 20 mM HEPES pH 7.5, 100 mM sodium chloride, 1.0% sodium cholate, 0.05% dodecylmaltoside, 5 mM beta-mercaptoethanol, and protease inhibitors. The solubilization reaction was stirred at 4 °C for 40 min, and then centrifuged to remove insoluble debris. Ni-NTA resin was added to the supernatant and stirred for 1.5 h at 4 °C followed by multiple washes of the Ni-NTA resin in batch with solubilization buffer. The resin was collected into a wide-bore glass column, and the detergent was gradually exchanged from sodium cholate to 0.1% dodecylmaltoside. The protein was eluted with Ni-NTA elution buffer (20 mM HEPES pH 7.5, 100 mM sodium chloride, 0.1% dodecylmaltoside, 5 mM beta-mercaptoethanol, 200 mM imidazole and protease inhibitors). To cleave off the amino terminal histidine tag, 3C protease (1:1000 w/w) was added and the sample dialyzed overnight in 20 mM HEPES pH 7.5, 100 mM sodium chloride, 0.1% dodecylmaltoside, 5 mM beta-mercaptoethanol, and 5 mM imidazole. The cleaved histidine tag, uncleaved fractions, and 3C protease were removed by incubation of the sample with Ni-NTA resin for 45 min at 4 °C. The slurry was loaded into a glass column and the flow-through containing the Gβγ heterodimer was collected. Lambda protein phosphatase (2000 units, NEB), calf intestinal phosphatase (10 units, NEB), and Antarctic phosphatase (5 units, NEB) were added together with 1 mM manganese chloride, followed by a 1 h incubation at 4 °C. After adjusting the sodium chloride concentration to 50 mM using dilution buffer composed of 20 mM HEPES pH 7.5, 0.02% dodecylmaltoside, and 1 mM DTT, the sample was passed through a 0.22 μm filter and loaded onto a MonoQ 10/100 GL column (GE Healthcare) equilibrated in buffer A (20 mM HEPES pH 7.5, 50 mM sodium chloride, 0.02%

12

dodecylmaltoside, and 1 mM DTT). The column was washed with 5 CV of buffer A and bound protein was eluted over 7.5 CV with a linear gradient from 0–25% buffer B (buffer A with 1 M sodium chloride). The fractions containing prenylated heterodimer were pooled, concentrated, and loaded onto a G50 column to remove reducing agents and exchange the protein into deuterated buffer (20 mM HEPES pH 7.5, 100 mM sodium chloride, 0.02% dodecylmaltoside). After concentrating the protein, 20% deuterated glycerol (Cambridge Isotopes) was added and protein aliquots were flash frozen in liquid nitrogen.

Site-directed spin labeling

For site-directed spin labeling, the Gα protein was loaded onto a Superdex 200 10/300 GL and eluted in labeling buffer (20 mM MOPS pH 6.8, 100 mM sodium chloride, 1 mM magnesium chloride, and 20 μM GDP). The main peak was collected and the protein was incubated with (1-Oxyl-2,2,5,5-tetramethylpyrroline-3-methyl) methanethiosulfonate (MTSSL, Enzo Life Sciences) in a 2:1 label:protein molar ratio for 15 min at room temperature. The labeling mixture was loaded onto a Sephadex G50 column equilibrated with deuterium buffer (20 mM HEPES pH 7.5, 100 mM sodium chloride, 1 mM magnesium chloride, and 20 μM GDP) to remove non-reacted spin label and exchange the buffer for DEER measurements. The protein was concentrated to 400 μM and shock frozen in liquid nitrogen after the addition of 20% deuterated glycerol (Cambridge Isotopes).

DEER measurements

Prior to collecting DEER dipolar evolution spectra, spin-labeled Gα subunits were mixed with Gβγ in a molar ratio of 1:1.2 and incubated for 30 min on ice to reconstitute the G protein heterotrimer. Subsequently, the sample was loaded into quartz capillaries and flash frozen in liquid nitrogen. DEER measurements were performed at 80 K on a Bruker ELEXSYS 580 spectrometer equipped with a ER 5107 D 2 Q-band resonator, a SuperQFT Q-band bridge and a

10-W AmpQ Q-band amplifier as previously described (*30*). Deuterated sample buffer and glycerol were used to achieve dipolar evolution times of 5.2 µs. Nuclear modulations caused by deuterium were suppressed by an eight-step nuclear modulation averaging cycle with 16 ns increments (*31*). DEER traces were analyzed with the software package LongDistances, written in LabVIEW and available at https://sites.google.com/site/altenbach/labview-programs/epr-programs and plotted using GraphPad Prism 6.0. The upper limits for obtaining accurate mean distances ($r_{\mathrm{max},\langle r\rangle}$) and accurate widths of the distance distribution ($r_{\mathrm{max},\langle\sigma\rangle}$) were calculated using the equations: $r_{\mathrm{max},\langle r\rangle} \approx 5\sqrt[3]{t_{\mathrm{max}}/(2\ \mu\mathrm{s})}$ nm and $r_{\mathrm{max},\langle\sigma\rangle} \approx 4\sqrt[3]{t_{\mathrm{max}}/(2\ \mu\mathrm{s})}$ nm (*31*).

Simulation of distance distributions

Spin label distance distributions corresponding to GDP-bound crystal structures were simulated using the MMM 2014 software (*32*) and X-ray structures of G_i heterotrimer bound to GDP (PDB entry 1GP2) (*5*) and $G\alpha_s$ in complex with GTPγS (PDB entry 1AZT) (*33*). Significantly populated spin label rotamers at the labeling sites were calculated using the Monte Carlo/United Force Field rotamer library for MTSSL at 175 K. The resulting interspin distance distributions were plotted using GraphPad Prism 6.0.

Nucleotide-Exchange Experiments

Expression and purification of heterotrimeric G proteins for nucleotide-exchange experiments

Heterotrimeric G_i was expressed in *Hi5* insect cells using baculoviruses generated by the BestBac (Expression Systems) method. We expressed the heterotrimeric G protein using two separate viruses; one virus delivers sequence for the human $G\alpha_i$ subunit and the other expresses the Gβ and Gγ subunits, as described above. The sequence for the Gβ subunit contains an amino terminal 6x histidine tag followed by a rhinovirus 3C protease sequence, allowing us to cleave

off the histidine tag after purification. *Hi5* cells were infected at a density of 3.0×10^6 cells/ml

and incubated at 27 °C for 48 h. After centrifugation, cells were lysed in a buffer comprised of

10 mM Tris, pH 7.5, 100 µM magnesium chloride, 5 mM beta-mercaptoethanol, 50 µM GDP,

and protease inhibitors. The membrane fraction was collected by centrifugation and solubilized

by a dounce homogenizer with a buffer comprised of 20 mM HEPES pH 7.5, 100 mM sodium

chloride, 1.0% sodium cholate, 0.05% dodecylmaltoside, 5 mM magnesium chloride, 5 mM

beta-mercaptoethanol, 50 µM GDP, and protease inhibitors. The solubilization reaction was

allowed to proceed for 45 min at 4 °C. The soluble fraction was incubated in batch with Ni-NTA

resin for 1.5 h at 4 °C followed by multiple washes of the Ni-NTA resin in batch with

solubilization buffer. The resin was loaded into a wide-bore glass column, and the detergent was

gradually exchanged from sodium cholate to 0.1% dodecylmaltoside. Heterotrimeric G protein

was eluted in buffer supplemented with 200 mM imidazole and dialyzed overnight in 20 mM

HEPES pH 7.5, 100 mM sodium chloride, 0.1% dodecylmaltoside, 1 mM magnesium chloride, 5

mM beta-mercaptoethanol, 50 µM GDP, and 5 mM imidazole. During dialysis, 3C protease

(1:1000 w/w) was added to the dialysis cassette to cleave off the amino terminal histidine tag. In

order to remove the cleaved histidine tag, uncleaved fractions, and 3C protease, the protein was

incubated in batch with Ni-NTA resin for 45 min at 4 °C. Then the slurry was loaded into a

wide-bore glass column and the flow-through containing heterotrimeric G protein was collected.

Lambda protein phosphatase (2000 units, NEB), calf intestinal phosphatase (10 units, NEB), and

Antarctic phosphatase (5 units, NEB) were added together with 1 mM manganese chloride

followed by incubation on ice for 1 h. After two-fold dilution with buffer composed of 20 mM

HEPES pH 7.5, 100 µM magnesium chloride, 0.02% dodecylmaltoside, and 100 µM TCEP, the

sample was passed through a 0.22 µm filter and loaded onto a MonoQ 10/100 GL column (GE

Healthcare) equilibrated in buffer A (20 mM HEPES pH 7.5, 50 mM sodium chloride, 100 µM

magnesium chloride, 0.02% dodecylmaltoside, and 100 µM TCEP). The column was washed

with 5 CV of buffer A at 2 ml/min and the G protein heterotrimer was eluted over 7.5 CV with a

linear gradient from 0–25% buffer B (buffer A with 1 M sodium chloride). The main peak

containing prenylated G protein heterotrimer was collected and GDP was added to 20 µM. After

dialyzing in 20 mM HEPES pH 7.5, 100 mM sodium chloride, 0.02% dodecylmaltoside, 100 μM TCEP, and 20 μM GDP, glycerol was added to 20% and the protein was concentrated to at least 20 mg/ml. The concentrated protein was then aliquoted, flash frozen in liquid nitrogen and stored at −80 °C until needed.

Measurement of nucleotide-exchange kinetics

For nucleotide-exchange experiments, BODIPY-FL-GTPγS fluorescence was measured with a Horiba FluoroMax-3 spectrofluorometer. The fluorophore was excited at 495 nm and emission was detected at 508 nm. Slit widths were set to 4 nm. All experiments were performed in a buffer comprised of 20 mM HEPES, pH 7.5, 100 mM sodium chloride, 0.02% dodecylmaltoside, 100 μM magnesium chloride, and 100 μM TCEP at 25 °C. Typically, kinetics data were collected for 30–150 nM BODIPY-FL-GTPγS in the absence of G protein for 100 s to establish the baseline fluorescence intensity. G protein constructs were added to 100 nM and rapidly mixed in the fluorescence cuvette without halting data collection. For the fast association kinetics observed for wild-type G_i, data points were acquired every second for 400 s. For the slower association kinetics observed for G_i-HD-tether construct, data points were acquired every 10 s to minimize photobleaching. The resulting kinetics spectra were plotted and fit to a one-phase association function using GraphPad Prism 6.0.

Table S1. Simulations

#	Duration (μs)	Protein	Ligand	Membrane	Opening-limiting restraints	TAMD	Receptor-mimicking restraints
1	6.4	G_t	GDP	Yes	-	-	-
2	25.3	G_t	GDP	Yes	-	-	-
3	2.2	G_t	GDP	Yes	-	-	-
4	10.0	G_t	GDP	-	-	-	-
5	10.0	G_t	GDP	-	-	-	-
6	5.0	G_t	GDP	-	-	-	-
7	5.0	G_t	GDP	-	-	-	-
8	10.0	G_t	GDP	-	-	-	-
9	10.0	G_t	GDP	-	-	-	-
10	10.0	G_t	-	-	-	-	-
11	25.0	G_t	-	-	-	-	-
12	7.9	G_t	-	-	-	-	-
13	10.0	G_t	-	-	-	-	-
14	10.0	G_t	-	-	-	-	-
15	10.0	G_t	-	-	-	-	-
16	14.0	G_t	GMP	-	-	-	-
17	10.0	G_t	GMP	-	-	-	-
18	10.0	G_t	GMP	-	-	-	-
19	10.0	G_t	PPi	-	-	-	-
20	10.0	G_t	PPi	-	-	-	-
21	10.0	G_t	PPi	-	-	-	-
22	50.0	$\beta_2AR–G_s$	-	Yes	-	-	-
23	10.0	$\beta_2AR–G_s$	-	Yes	-	-	-
24	10.0	$\beta_2AR–G_s$	-	Yes	-	-	-
25	10.0	G_t	Fos	-	-	-	-
26	5.0	G_t	Fos	-	-	-	-
27	10.0	G_i	GDP	-	-	-	-
28	10.0	G_i	GDP	-	-	-	-
29	10.0	G_i	GDP	-	-	-	-
30	12.1	G_i	GDP	-	-	-	-
31	25.0	G_t	GMP	-	Tight	-	-
32	10.0	G_t	GMP	-	Tight	-	-
33	25.0	$G_t\Delta HD$	GDP	-	-	-	-
34	2.2	$G_t\Delta HD$	GMP	-	-	-	-
35	0.5	$G_t\Delta HD$	GMP	-	-	-	-
36	0.5	$G_t\Delta HD$	GMP	-	-	-	-
37	3.1	$G_t\Delta HD$	GDP	-	-	Yes	
38	5.0	$G_t\Delta HD$	GDP	-	-	Yes	-
39	3.0	$G_t\Delta HD$	GDP	-	-	Yes	Yes
40	0.2	$G_t\Delta HD$	GDP	-	-	Yes	Yes

41	1.0	$G_t\Delta HD$	GDP	-	-	Yes	Yes
42	0.5	$G_t\Delta HD$	GDP	-	-	Yes	Yes
43	0.3	$G_t\Delta HD$	GDP	-	-	Yes	Yes
44	1.0	$G_t\Delta HD$	GDP	-	-	Yes	Yes
45	8.0	$G_t\Delta HD$	GDP	-	-	Yes	Yes; no $\alpha 5$
46	5.0	$G_t\Delta HD$	GDP	-	-	Yes	Yes; no $\alpha 5$
47	5.0	$G_t\Delta HD$	GDP	-	-	Yes	Yes; no $\alpha 5$
48	20.0	G_t	GDP	-	-	-	Yes
49	6.0	G_t	GDP	-	-	Yes	Yes
50	6.0	G_t	GDP	-	-	Yes	Yes
51	6.0	G_t	GDP	-	-	Yes	Yes
52	6.0	G_t	GDP	-	-	Yes	Yes
53	6.0	G_t	GDP	-	-	Yes	Yes
54	6.0	G_t	GDP	-	-	Yes	Yes
55	25.0	G_t	GDP	-	-	Yes	-
56	6.0	G_t	GDP	-	-	Yes	Yes
57	9.1	G_t	GDP	-	-	Yes	Yes
58	4.0	G_t	GDP	-	-	Yes	Yes
59	10.0	$G\alpha_t$	GTP/Mg^{2+}	-	-	-	-
60	10.0	$G\alpha_t$	GTP/Mg^{2+}	-	-	-	-
61	10.0	$G\alpha_t$	GTP/Mg^{2+}	-	-	-	-
62	20.0	G_t	GMP	-	Loose	-	-
63	17.2	G_t	GMP	-	Loose	-	-
64	7.0	G_t	GMP	-	Loose	-	-
65	5.0	β_2AR–G_s	-	Yes	-	-	-
66	10.0	$G_t\Delta HD$	GDP	-	-	Yes	-

Proteins simulated were heterotrimeric G proteins G_t ($G\alpha_{ti}\beta_1\gamma_1$, a transducin chimera), G_s ($G\alpha_s\beta_1\gamma_2$), G_i ($G\alpha_{i1}\beta_1\gamma_2$), and $G_t\Delta HD$ (the transducin chimera with its helical domain removed); monomeric $G\alpha_t$ (the chimeric α subunit); and the β_2-adrenergic receptor (β_2AR) (see *Initial coordinates and system setup* in *Molecular Dynamics Simulations*). Ligands were guanosine mono-, di-, and tri-phosphate (GMP, GDP, and GTP, respectively), pyrophosphate (PPi), and the pyrophosphate-mimetic foscarnet (Fos). Certain simulations included a membrane; in these simulations, lipid modifications to the proteins (which serve as membrane anchors) were also included. Simulations 22–24 used the long isoform of $G\alpha_s$, while simulation 65 used the short isoform. In several simulations, an α subunit interdomain distance was restrained in order to eliminate opening entirely or to allow only limited opening (see *Opening-limiting restraints*). To study GDP dissociation, TAMD was applied to accelerate motion of the center of mass of the

non-hydrogen atoms of GDP (see *Temperature-accelerated molecular dynamics*); TAMD simulations 49–58 were initialized by randomizing the velocities of a frame from simulation 48 near 10 μs. Finally, to mimic the effect of a receptor, certain atoms were restrained to the positions of corresponding atoms in the β_2AR–G_s crystal structure (see *Receptor-mimicking restraints* and *Temperature-accelerated molecular dynamics* in Materials and Methods).
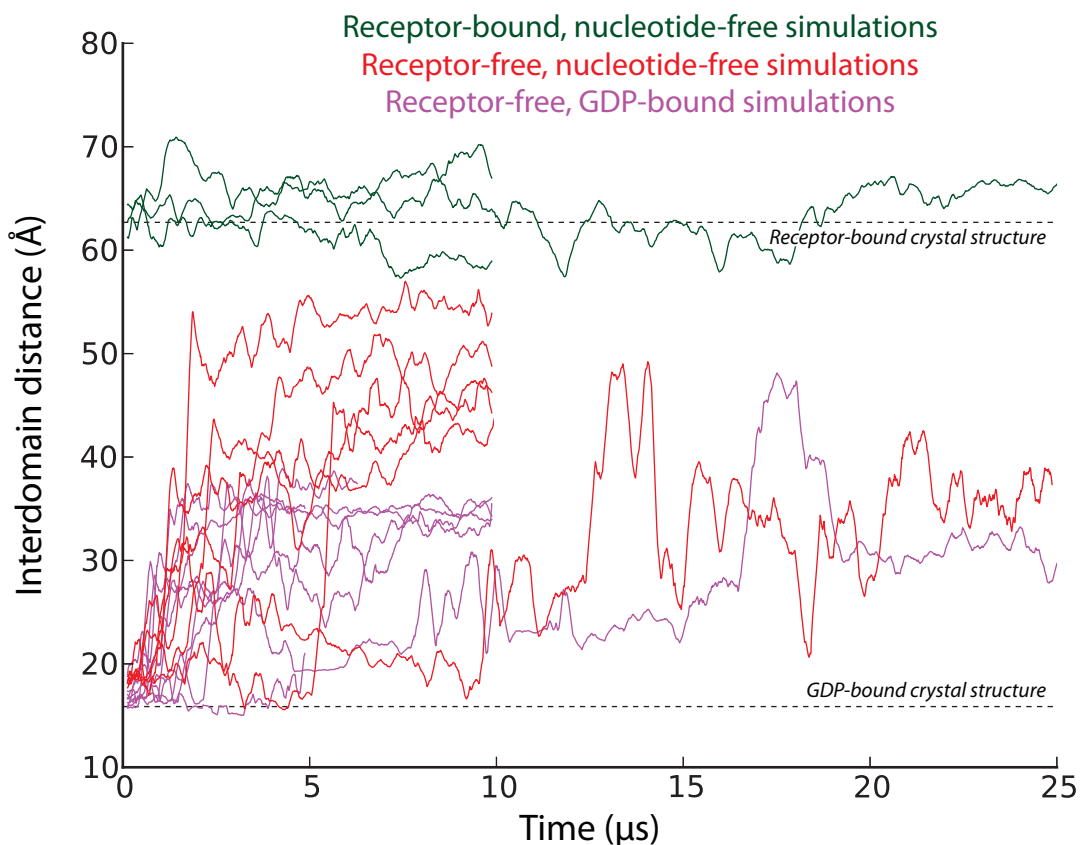
Figures

Figure S1. The time traces of the interdomain distance shown in Figs. 1C and 3A from additional simulations. Distances were computed between the α carbons of α subunit residues 134 and 272 (G_t) or 161 and 299 (G_s). For clarity, only 250-ns moving averages are shown. Distances from crystal structures are shown for comparison. Data are from simulations 1–9 of Table S1 (receptor-free, GDP-bound G_t), 10–15 (receptor-free, nucleotide-free G_t), and 22–24 (receptor-bound, nucleotide-free G_s).
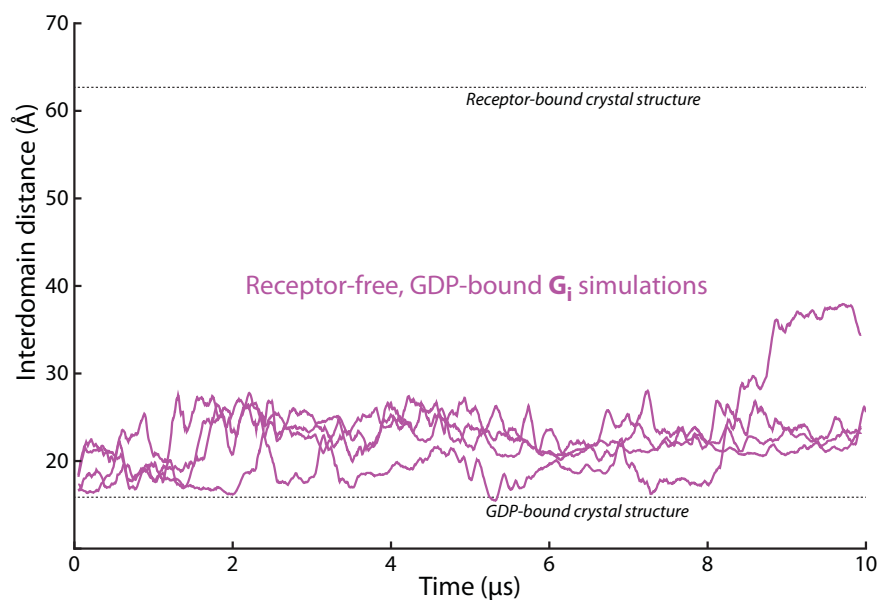
Figure S2. Time traces of interdomain distances in GDP-bound simulations of G_i. Distances were computed between the α carbons of α subunit residues 138 and 276, which correspond to residues 134 and 272 in G_t. Comparison of these traces to the GDP-bound G_t simulations shown in Figs. 1C and S1 indicates that both G_t and G_i undergo substantial domain separation even with GDP bound, although domain separation tends to take place more quickly in G_t. Data shown here are from simulations 27–30. For clarity, only 100-ns moving averages are shown. Distances from the crystal structures of the nucleotide-free $β_2AR$–G_s complex (PDB entry 3SN6) and GDP-bound heterotrimer (PDB entry 1GP2 for G_i and PDB entry 1GOT for G_t; the corresponding distances in these two structures differ by only ~0.5 Å) are shown for comparison.
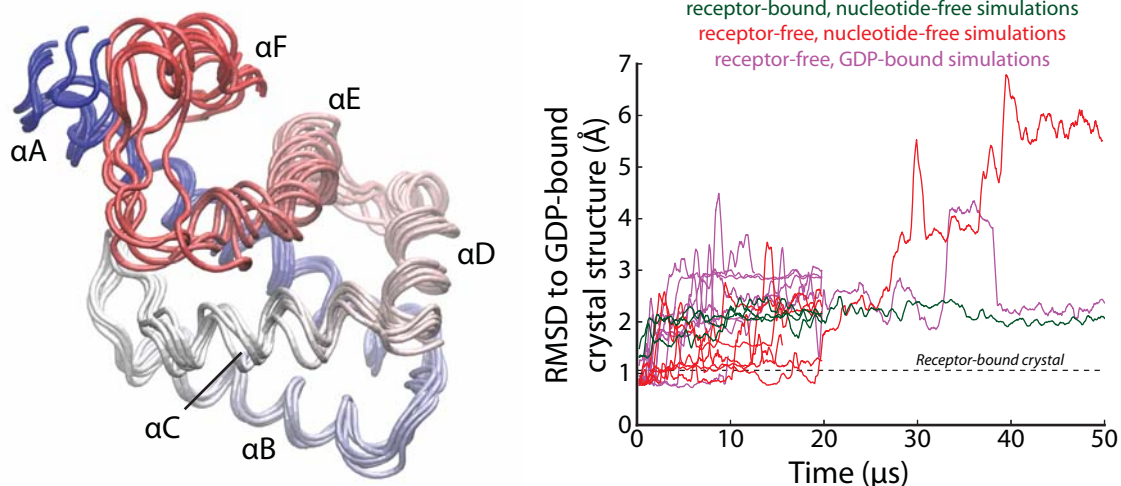
Figure S3. The helical domain is mostly rigid in simulation. Left, the helical domain at multiple time points during a simulation of GDP-bound G_t (simulation 9 at 0, 1, 2, 3, 4, and 5 μs), aligned on the helical domain itself. Although the helical domain flops around relative to the Ras domain, it maintains its internal structure (the overall flopping motion is not visible here due to the alignment). In some simulations, the region around αA and αF is unstable, as shown here. Right, time traces of the root-mean-square deviation (RMSD) of the helical domain helices in simulations from their conformation in the GDP-bound crystal structure. The α carbons from residues 63–86, 95–107, 117–141, 147–160, and 167–173 ($α_t$) or residues 89–112, 123–135, 144–168, 174–187, and 194–200 ($α_s$) were aligned to their positions in the GDP-bound G_t crystal structure, and RMSDs were computed on these atoms. Data are from the same simulations as in Fig. S1.
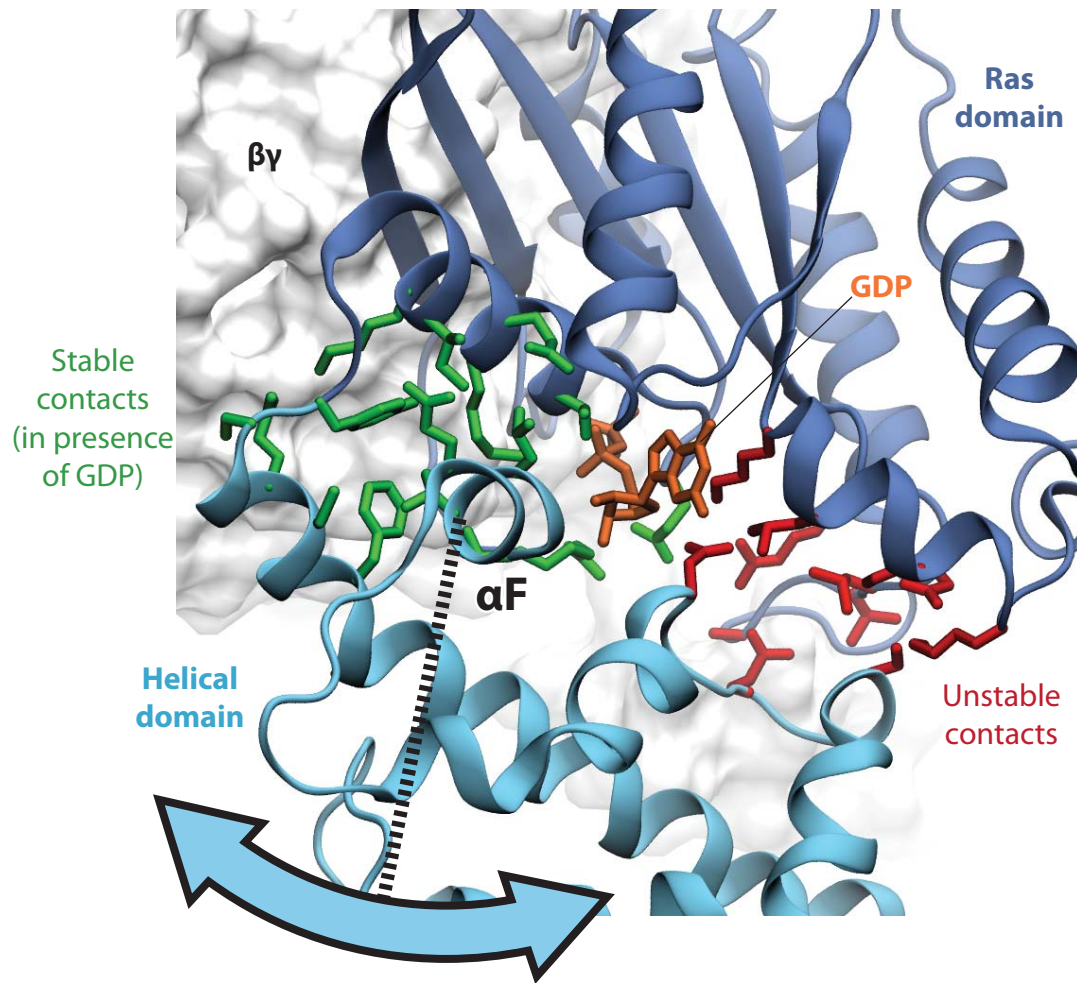
Figure S4. In the GDP-bound α subunit, the helical domain swings in such a way that the αF helix remains docked against the Ras domain in roughly the same place. The interdomain contacts shown in green are stable in simulations of GDP-bound G_t (but rearrange and often break in simulations where GDP is removed). The interdomain contacts shown in red are unstable in simulations of GDP-bound G_t.
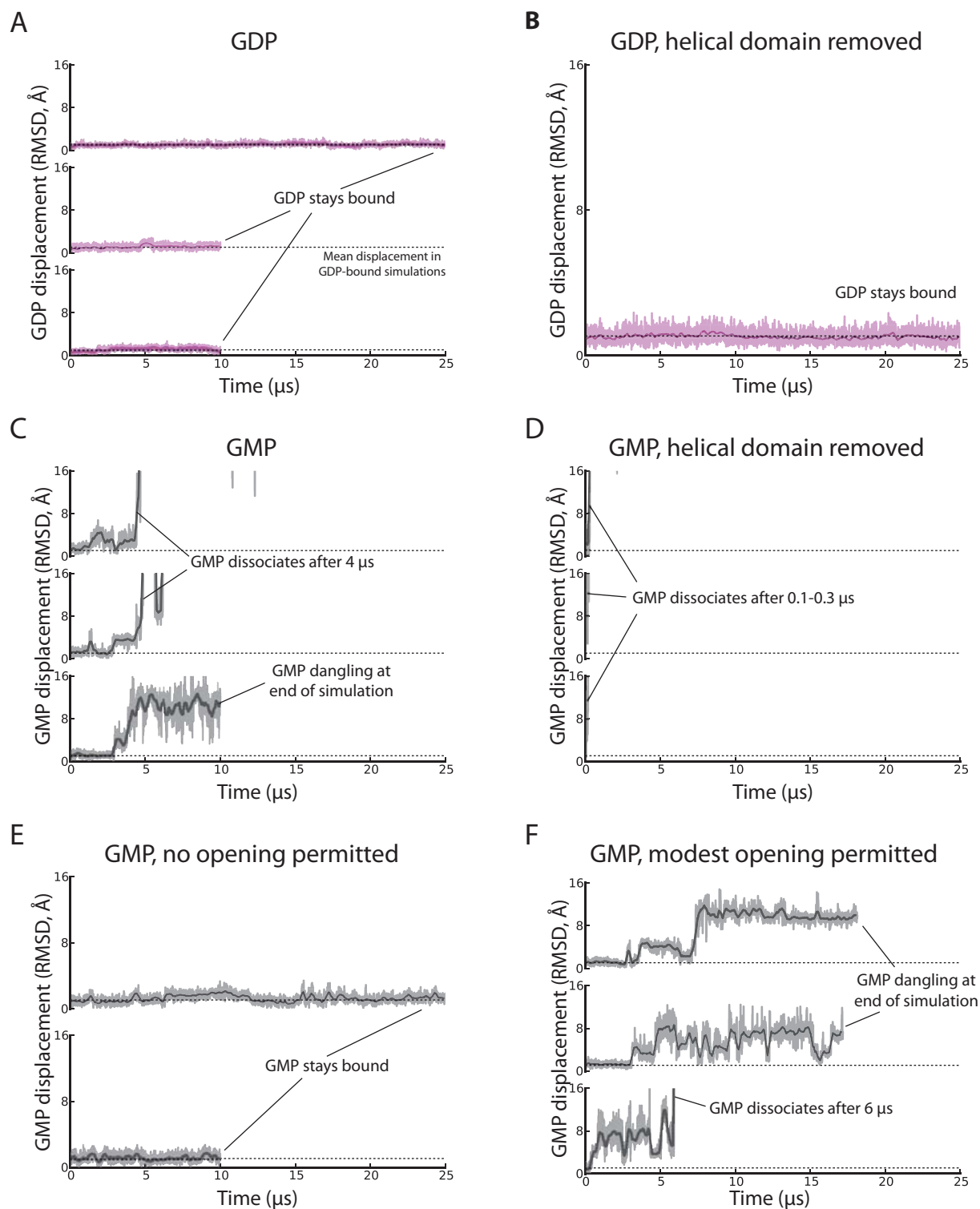
Figure S5. Rapid GDP dissociation requires both domain separation and disruption of interactions between GDP and the Ras domain. (A) GDP stays tightly bound in simulations of

the GDP-bound G_t heterotrimer (simulations 2, 5, and 8 are shown). Mean GDP displacement from the crystallographic position under this condition is shown as a dashed horizontal line in all plots in this and other panels. (B) GDP stays tightly bound to the Ras domain in a simulation where the helical domain (residues 58–174) was removed completely (simulation 33). (C) GMP unbinds from G_t within a few microseconds (simulations 16–18). (D) GMP unbinds rapidly (within 100–300 ns) in simulations where the helical domain is removed (simulations 34–36). (E) GMP does not unbind in simulations in which separation of the helical and Ras domains is prevented by artificial restraints (simulations 31 and 32). (F) GMP unbinds if the helical domain is allowed to separate from the Ras domain by up to 15 Å (top trace; simulation 62) or 25 Å (bottom traces; simulations 63 and 64), as measured by the increase in distance between the Cα atoms of Ala134 and Glu272 relative to the GDP-bound G_t heterotrimer crystal structure. See Materials and Methods for details.
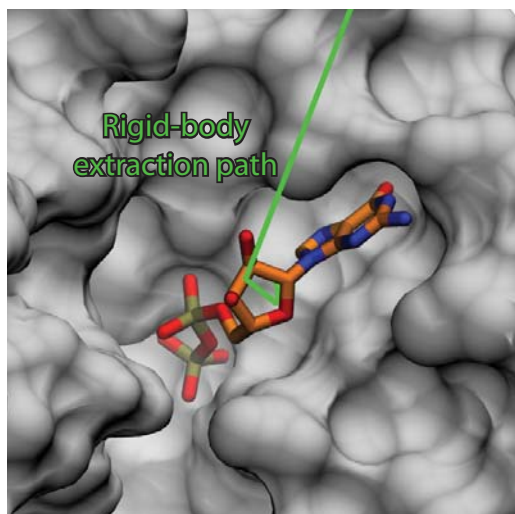
Figure S6. The open α subunit conformations seen in GDP-bound G protein simulations provide a clear exit pathway for GDP. In particular, we found many simulation snapshots in which the GDP could be moved from its position in the nucleotide-binding pocket to the bulk solvent without any steric clashes, even if the GDP and the protein were each held rigid in the conformation seen in the snapshot. To test whether GDP could be extracted as a rigid body from a particular simulation frame, random translations and rotations were generated and applied to move GDP as a rigid body, with individual atoms moving up to 0.1 Å per iteration. Moves were accepted if no GDP atom ended up in a steric clash with protein (as defined by two atoms within 80% of the sum of their van der Waals radii.) Above, the resulting trajectory of the GDP centroid is indicated as a green trace. The configuration is from simulation 5 around 1.692 μs and has an interdomain distance (Ala134–Glu272) of about 35 Å.

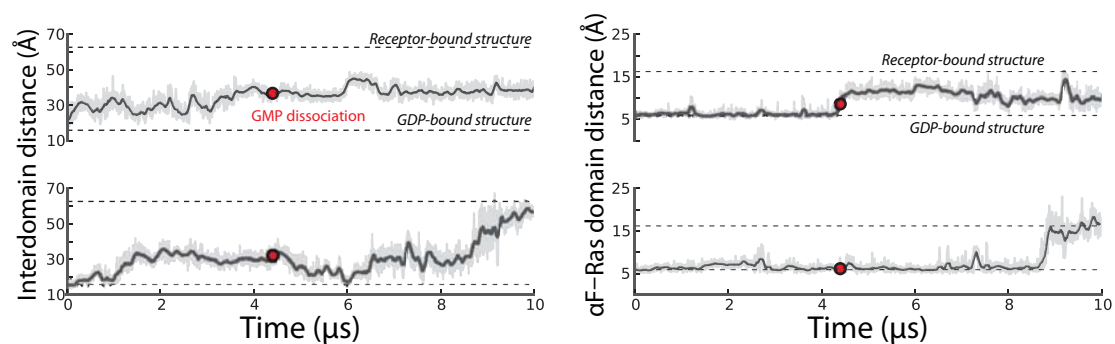## Unbiased, receptor-free, GMP-dissociation simulations

Figure S7. GMP dissociates only after the Ras and helical domains have separated, and GMP dissociation is followed by dislocation of the αF helix. The left-hand traces show interdomain distance, as measured between the Cα atoms of Ala134 and Glu272, as a function of simulation time for two simulations of the G$_t$ heterotrimer initiated with GMP in the nucleotide-binding site (simulations 16 and 17). The right-hand traces show the distance between the αF helix and the Ras domain, as measured between the Cα atoms of Thr44 in the Ras domain and Leu171 on the αF helix, for the same two simulations.
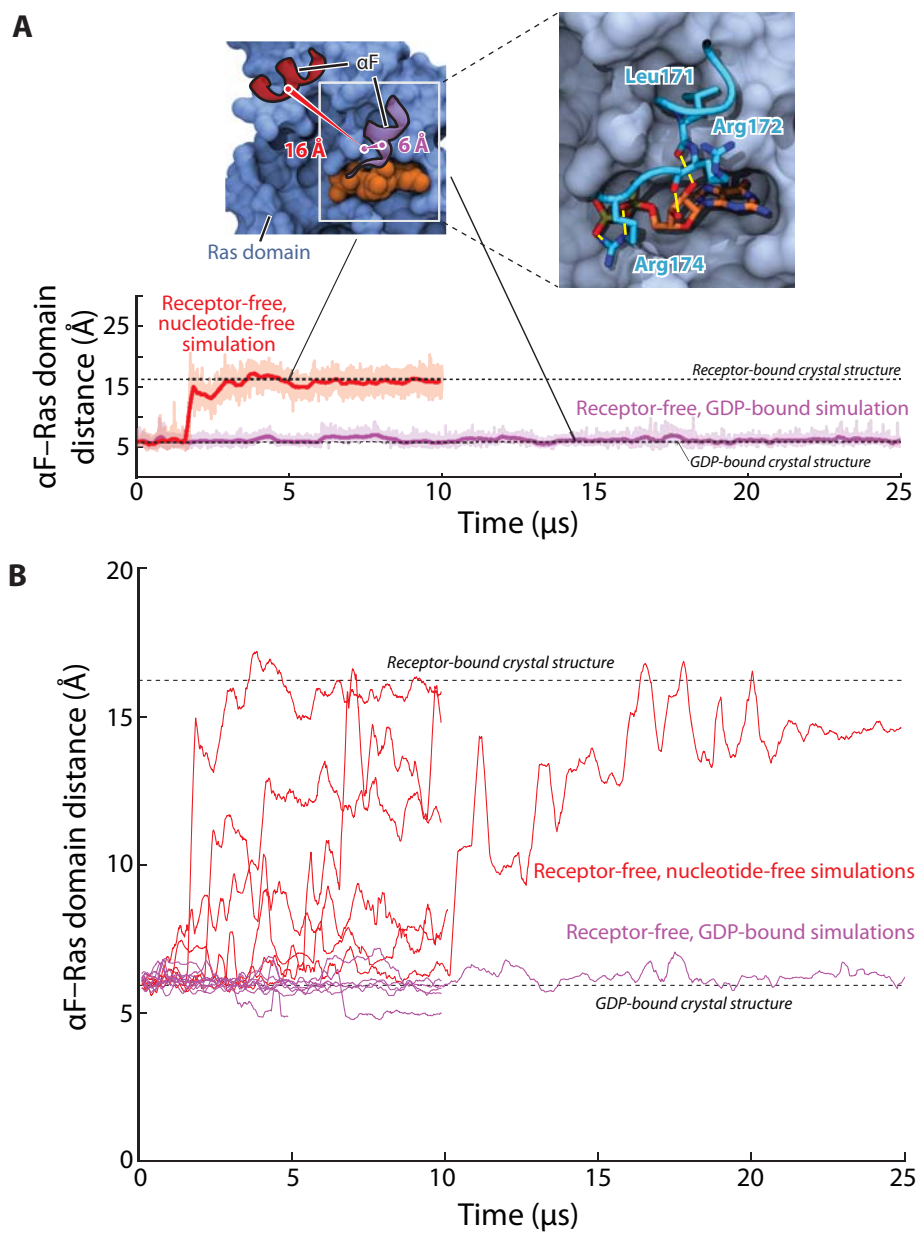
Figure S8. Helical domain helix αF dislocates in the absence of nucleotide, allowing greater domain separation. (A) When GDP is bound, αF and the Ras domain α1 helix together cradle the nucleotide ribose-α-phosphate group, and Arg174, which is near αF, often forms a salt bridge with the nucleotide phosphates. Helix αF—the domain separation joint—remains in contact with α1 as long as GDP is bound (GDP; right snapshot), as demonstrated by the Thr44–Leu171 inter-helical distance (trace). In the absence of nucleotide, however, αF unpacks from α1, moving ~10 Å away (left snapshot). Raw (light colors) and smoothed (250-ns moving average; dark colors)

data are shown. Data are from simulations 2 and 14 (Table S1). (B) Time traces of the distance between the Cα atoms of Thr44 (in the Ras domain) and Leu171 (in αF) show that αF is stably docked on the Ras domain in all GDP-bound G_t heterotrimer simulations (purple traces; simulations 1–9). When GDP is removed (red traces; simulations 10–15), the αF helix displaces. Corresponding distances from crystal structures are shown for comparison.
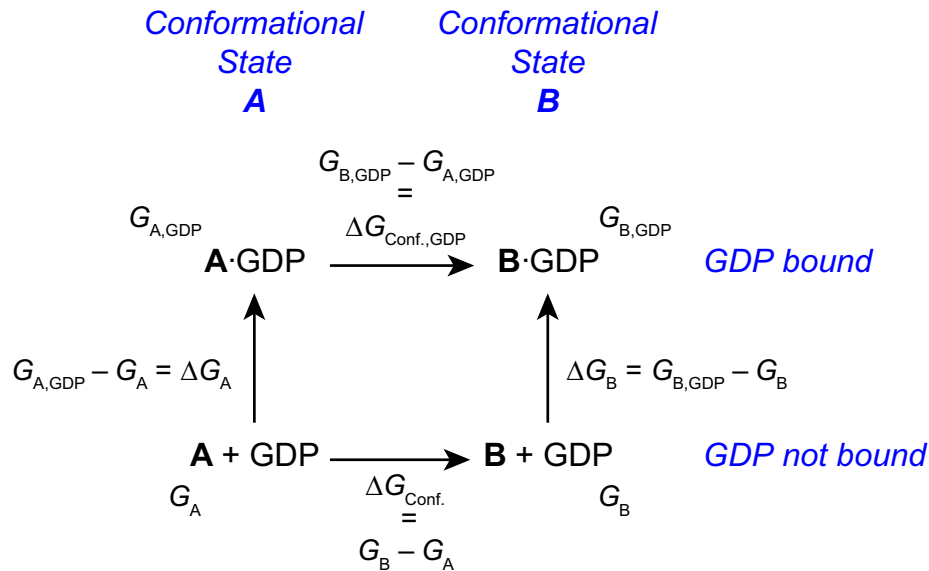
Conformational State A   *Conformational State B*

$$G_{\text{B,GDP}} - G_{\text{A,GDP}} = \Delta G_{\text{Conf.,GDP}}$$

$G_{\text{A,GDP}}$ $G_{\text{B,GDP}}$

A·GDP $\xrightarrow{\Delta G_{\text{Conf.,GDP}}}$ **B**·GDP   *GDP bound*

$G_{\text{A,GDP}} - G_{\text{A}} = \Delta G_{\text{A}}$ $\Delta G_{\text{B}} = G_{\text{B,GDP}} - G_{\text{B}}$

A + GDP $\xrightarrow{\Delta G_{\text{Conf.}}}$ **B** + GDP   *GDP not bound*

G_{A} $\Delta G_{\text{Conf.}} = G_{\text{B}} - G_{\text{A}}$ G_{B}

Figure S9. Justification for the claim that "if affinity for GDP is weaker when the G protein adopts a particular conformation than when it does not, then removal of GDP will increase the equilibrium population of that conformation." We define state A as the "particular conformation"—or, more generally, set of conformations—of the G protein, and state B as the set of all other conformations, such that the G protein is always in either state A or state B. The free energies of states A and B, with and without GDP bound (at some reference concentration of GDP), are annotated as "G_{A}", "G_{B}", "$G_{\text{A,GDP}}$", and "$G_{\text{B,GDP}}$". By definition, the affinity for GDP is weaker in state A than in state B if and only if $\Delta G_{\text{A}} > \Delta G_{\text{B}}$. Similarly, the equilibrium population of state A is greater in the absence of GDP than in its presence if and only if $\Delta G_{\text{Conf.,GDP}} > \Delta G_{\text{Conf.}}$ Algebraic manipulation demonstratese that these two inequalities are in fact equivalent:

$$\Delta G_{\text{A}} > \Delta G_{\text{B}} \Leftrightarrow G_{\text{A,GDP}} - G_{\text{A}} > G_{\text{B,GDP}} - G_{\text{B}}$$

$$\Leftrightarrow G_{\text{B}} - G_{\text{A}} > G_{\text{B,GDP}} - G_{\text{A,GDP}}$$

$$\Leftrightarrow \Delta G_{\text{Conf.,GDP}} > \Delta G_{\text{Conf.}}$$

A Ras-domain residues contacting receptor in crystal structure

α5

Ras-domain residues mobilized by GDP removal

B Receptor-bound, nucleotide-free simulations
Receptor-free, nucleotide-free simulations
Receptor-free, GDP-bound simulations

RMSD to receptor-bound structure (Å)

α5 helix

GDP-bound crystal

Time (μs)

C

RMSD to receptor-bound structure (Å)

α5 helix

GDP-bound crystal

Extreme value

Mean from receptor-bound simulations

Time (μs)

D GDP-bound simulation
Receptor-bound structure

I339

F332

V328   N327

Extreme value

Figure S10. In several G_t simulations initiated from the nucleotide-bound structure but with GDP removed, the α5 helix rotated and translated into the conformation seen in the receptor-bound G_s structure. Similar conformations were also adopted in certain GDP-bound simulations, but far more rarely. (A) The α5 helix is the only receptor-interacting structural element in G_t whose conformation tends to change in simulation upon removal of GDP. Left: The G protein residues shown in yellow are the only Ras domain residues that contact the receptor in the receptor-bound crystal structure. Right: The G protein Ras domain residues shown in green are those whose position tends to shift upon removal of GDP. For each α carbon atom in the Ras domain, we computed the RMS distance of that atom's position in simulation from its position in the GDP-bound crystal structure. We did this for both receptor-free, GDP-bound simulations (simulations 1–9) and receptor-free, nucleotide-free simulations (simulations 10–15), and then computed the difference between the two cases. Larger differences (i.e., more displacement in

31

the absence of the nucleotide) correspond to bolder shades of green, with saturation at 4 Å. (B) Time traces of the RMSD of the α5 helix in various simulations to its position in the receptor-bound crystal structure, showing that in several simulations initialized from a receptor-free, GDP-bound G_t structure, but with the nucleotide removed, the α5 helix spontaneously adopted a position that closely matches that seen in the receptor-bound structure. RMSDs were computed on the α carbons of the α5 helix ($G\alpha_t$ residues 331–338/$G\alpha_s$ residues 375–382) after alignment of residues in strands β2–β6 to the receptor-bound crystal structure (PDB entry 3SN6). Data are from the same simulations as in Fig. S1, and the traces shown are moving averages over 250-ns windows. (C) Even in GDP-bound simulations, the α5 helix sometimes transiently approaches the position seen in the GPCR-bound crystal structure, but only rarely. One of the smoothed traces from panel C, for a GDP-bound simulation (simulation 2), is shown again here (dark purple), together with its unsmoothed version (light purple). In this simulation, the α5 helix adopts conformations within 1.5 Å of the receptor-bound structure, but such conformations were roughly 1,000 times more common in simulations where GDP was removed than in simulations where GDP was retained. (D) A typical conformation of the α5 helix in a GDP-bound simulation is shown at left, while a rarely visited conformation similar to that of the receptor-bound structure is shown at right. The purple structures are taken from simulation snapshots near 19.3 μs (left) and 21.7 μs (right; extreme value noted in panel C) in simulation 2. Mutation to alanine of the residues labeled in this panel was reported to accelerate both uncatalyzed and receptor-catalyzed nucleotide exchange in an alanine-scanning mutagenesis study using recombinant G_t (*34*). Mutations F332A and V328A have particularly dramatic effects (151-fold and 77-fold acceleration of uncatalyzed exchange, and 5-fold and 3-fold acceleration of receptor-catalyzed exchange, respectively). Structurally speaking, replacing F332, V328, or I329 with alanine appears to disrupt the hydrophobic packing of α5 against the β-sheet in the GDP-bound state, while replacing N327 with alanine disrupts hydrogen bonds formed by N327 in the GDP-bound state. In simulation, we observed a tendency of F332 to get jammed during rotation and translation of α5 (see rendering), which may explain the particularly strong effect of alanine substitution at this position. In contrast, alanine substitutions at conserved residues V331 and

I338 impaired receptor-catalyzed nucleotide exchange (*34*). Structurally, replacing these residues with alanine likely weakens the hydrophobic packing of α5 against the β-sheet in the receptor-bound conformation.
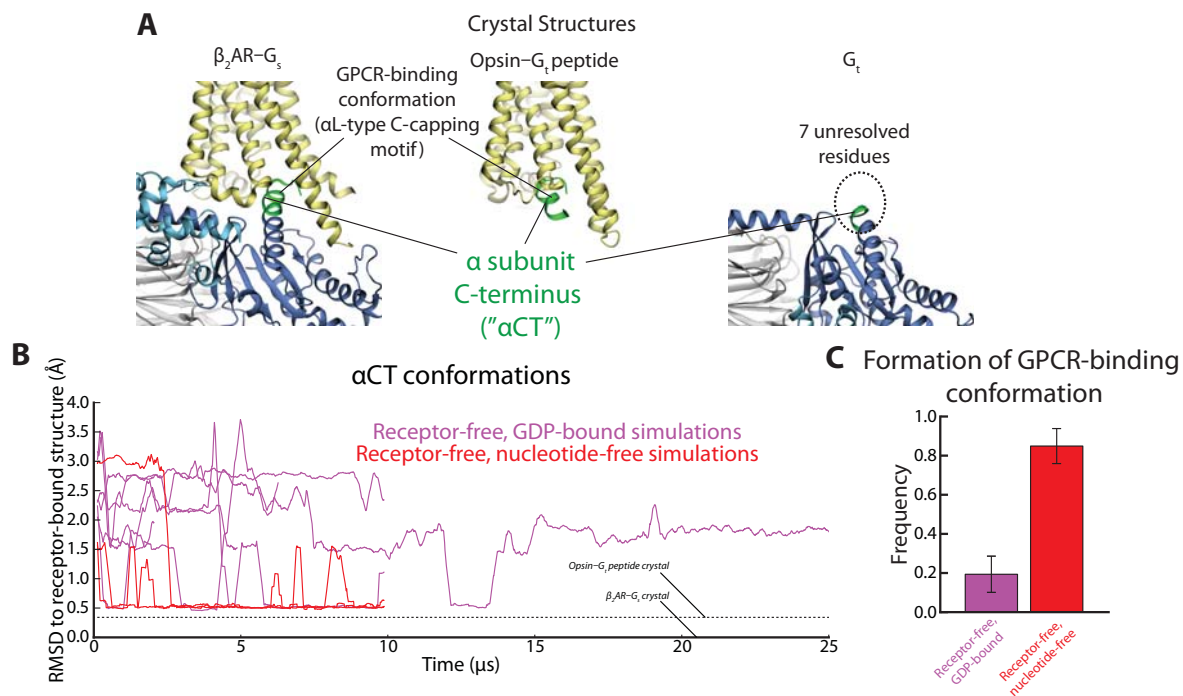
Figure S11. A GPCR-interacting conformation of the Gα C-terminus (an αL-type C-capping motif) forms spontaneously in receptor-free, nucleotide-free G_t simulations. It also forms occasionally in receptor-free, GDP-bound G_t simulations, but much less frequently. (A) The 11 C-terminal residues of the α subunit (αCT) form a well-defined conformation in crystal structures in complex with a receptor, but are disordered or unresolved in the absence of the receptor. Left, crystal structure of nucleotide-free G_s in complex with activated $β_2$ adrenergic receptor (PDB entry 3SN6.) Middle, crystal structure of the α subunit C-terminal peptide of G_t in complex with activated opsin (PDB entry 3DQB.) Right, crystal structure of a GDP-bound G_t heterotrimer (PDB entry 1GOT). (B) RMSD of αCT to the receptor-bound structure for several receptor-free simulations. Smoothed data (250-ns moving average) from simulations 1–6 and 13–15 are shown. RMSDs are computed on the α-carbons of αCT. (C) The GPCR-interacting conformation forms (RMSD < 1.0 Å) much more frequently in nucleotide-free simulations than in GDP-bound simulations. The bars indicate mean frequency and SEM for simulations 1–6 and 13–15.
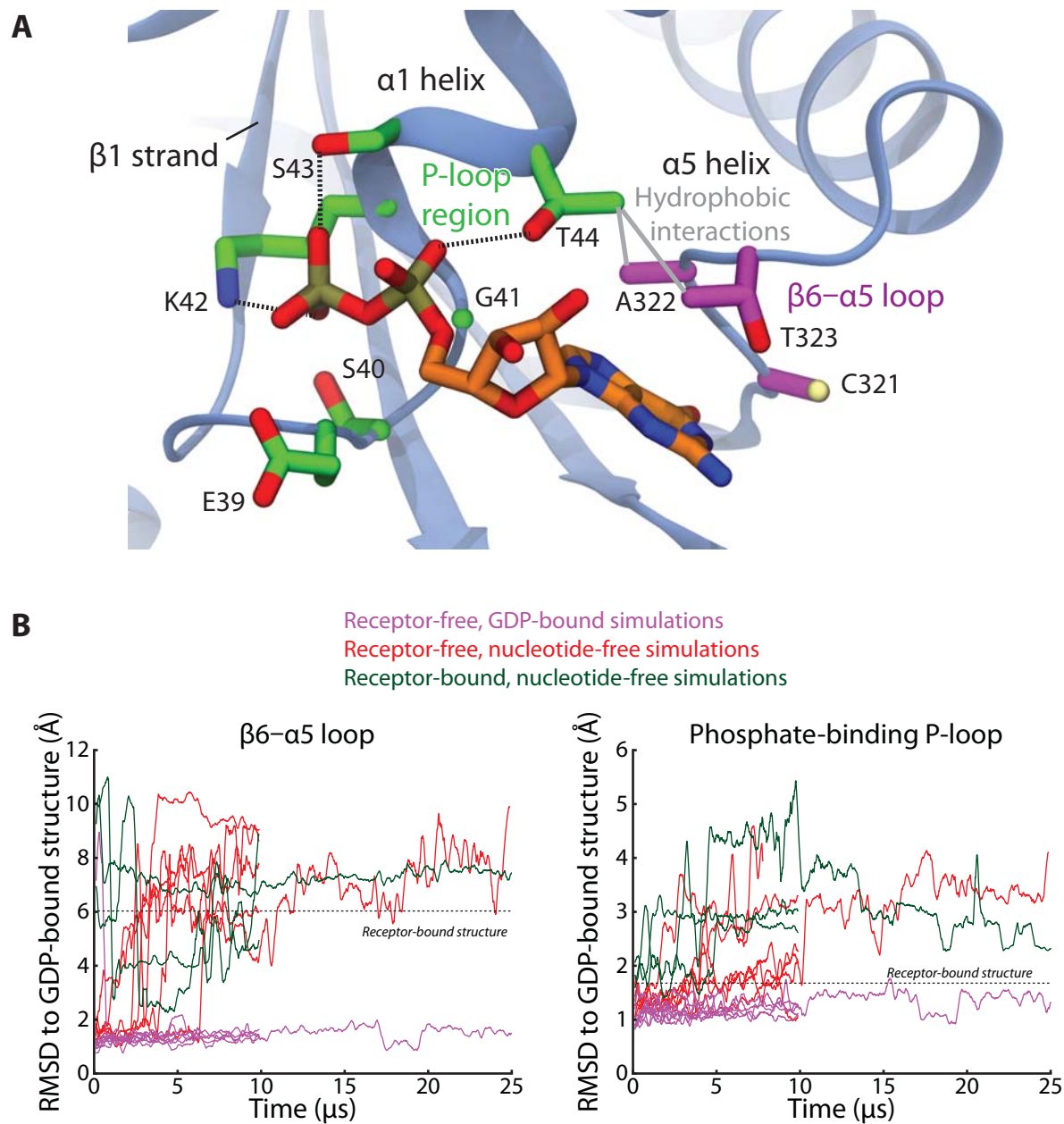
Figure S12. Two regions of the Ras domain's nucleotide-binding site are destabilized by the absence of GDP. (A) Illustration of GDP coordination; residue numbers are for G_t. The P-loop region (green residues) binds GDP at its phosphate moieties via a number of backbone hydrogen bonds and polar interactions with several side chains on the α1 helix. Residues on the β6–α5 loop (magenta) bind GDP at its guanine moiety via extensive van der Waals contact with a threonine side chain as well as a conserved hydrogen bonding network involving N265 and D268

on β5 and αG (not shown). The helical domain is omitted for clarity. The P-loop region and the β6–α5 loop are linked by hydrophobic interactions between T44 on the α1 helix and A322 and T323 on the β6–α5 loop; as a result destabilization of one region may affect the other region. The α1 and α5 helices are also linked by interactions between Q48, T325, and V328 (not shown). (B) Time traces of α-carbon RMSD to the GDP-bound crystal structure for the β6–α5 loop (left, G_t residues 321–323/G_s residues 365–367) and the P-loop region (right; G_t residues 39–44/G_s residues 50–55) for various simulations. To compute the RMSDs, structures were aligned to the GDP-bound G_t crystal structure (PDB entry 1GOT) using residues in strands β2–β6. Data are from the same simulations as in Fig. S1. Note: the receptor-bound crystal structure was determined in the presence of 10 mM foscarnet, a non-hydrolyzable pyrophosphate mimic, which may serve to stabilize the P-loop region.
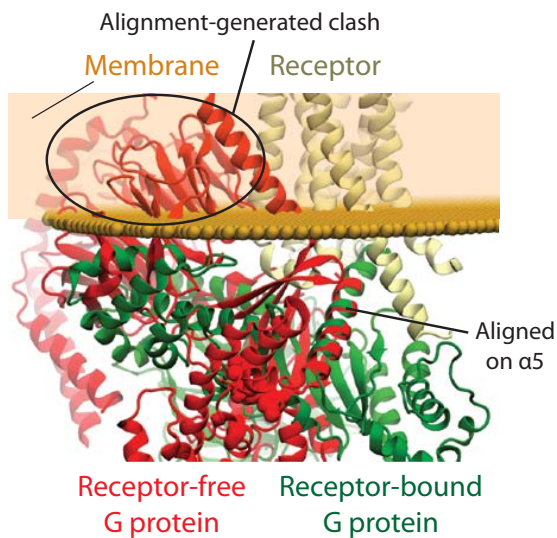
Figure S13. The α5 helix of a G protein must displace from the conformation seen in GDP-bound crystal structures in order to interact with a receptor as seen in the crystal structure of the β₂AR–Gₛ complex. If one positions the crystallographic GDP-bound Gₜ heterotrimer structure (red; PDB entry 1GOT) such that its α5 helix aligns with that of the β₂AR–Gₛ complex (green and yellow; PDB entry 3SN6), large parts of the GDP-bound G protein end up in the membrane (orange). The structures were aligned on α carbons from residues 325–343 (Gₜ) and 369–387 (Gₛ).
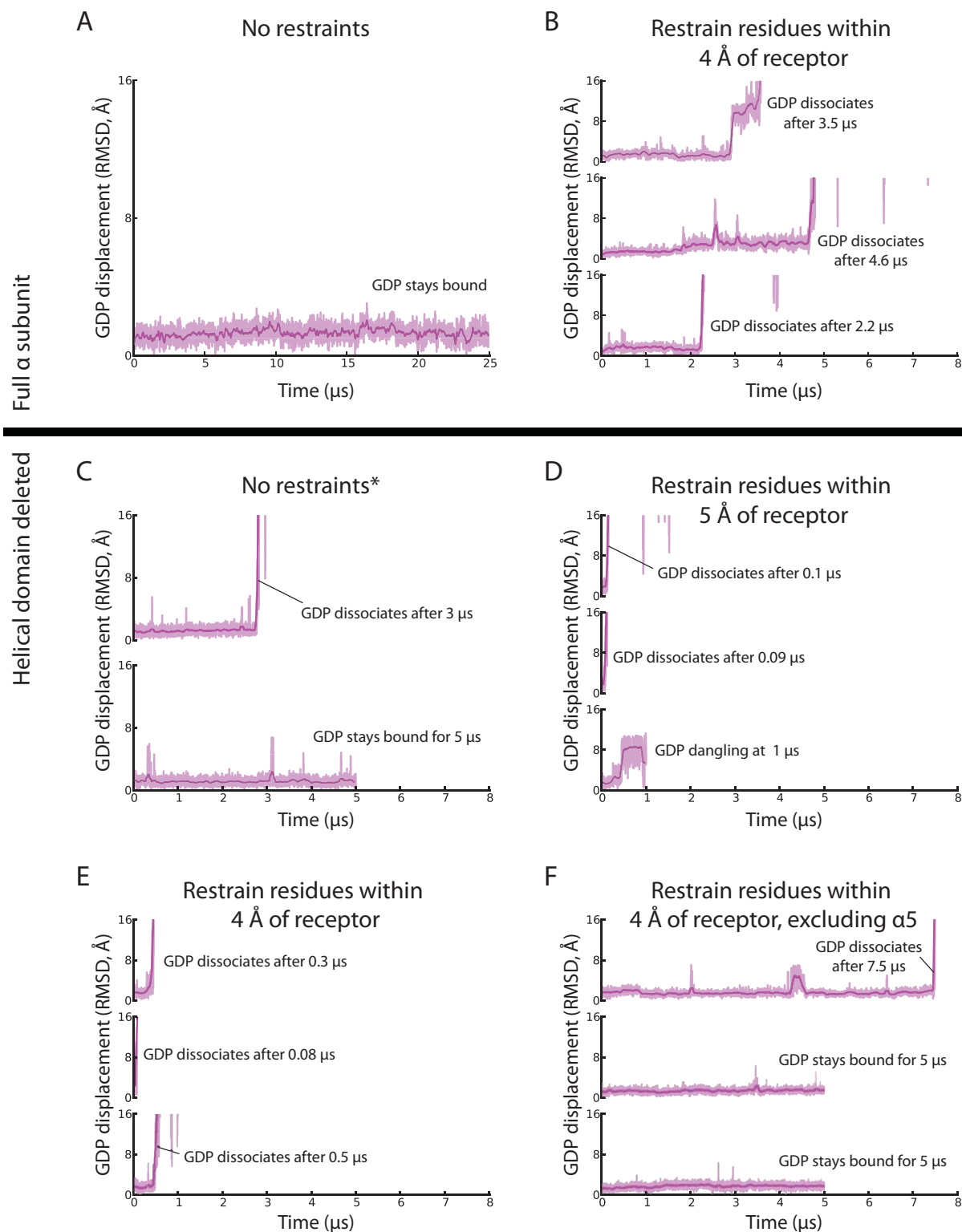
Figure S14. Restraining the α5 helix to the conformation seen in the β₂AR–Gs crystal structure promotes GDP release. Temperature-accelerated molecular dynamics simulations of GDP-

bound G_t were performed with (A, B) and without (C–F) the helical domain (α subunit residues 58–174), beginning with the protein and GDP in the conformation seen in the GDP-bound, receptor-free crystal structure (PDB entry 1GOT). Acceleration was applied to the GDP center of mass, in order to allow observation of GDP release on computationally accessible timescales (see Materials and Methods). Restraints were applied in certain simulations to target (push) receptor-proximal residues to the positions of the homologous residues in the β₂AR–G_s crystal structure (PDB entry 3SN6). Gα residues that are within 4 Å of the receptor in the β₂AR–G_s structure were restrained in (B) and (E); residues within 5 Å of the receptor were restrained in (D); and residues within 4 Å of the receptor but not on the α5 helix were restrained in (F). We saw much faster GDP dissociation in simulations with restraints on the α5 helix (B, D, E) than in those without (A, C, F). The asterisks in C refer to the fact that residues 30, 186, 191, 216, 260, and 316, all in the Ras domain's β sheet, were restrained to ensure that acceleration of the nucleotide did not lead to overall motion of the protein. See Materials and Methods for details. Simulations shown: A) 55, B) 56–58, C) 37, 38, D) 39–41, E) 42–44, and F) 45–47.
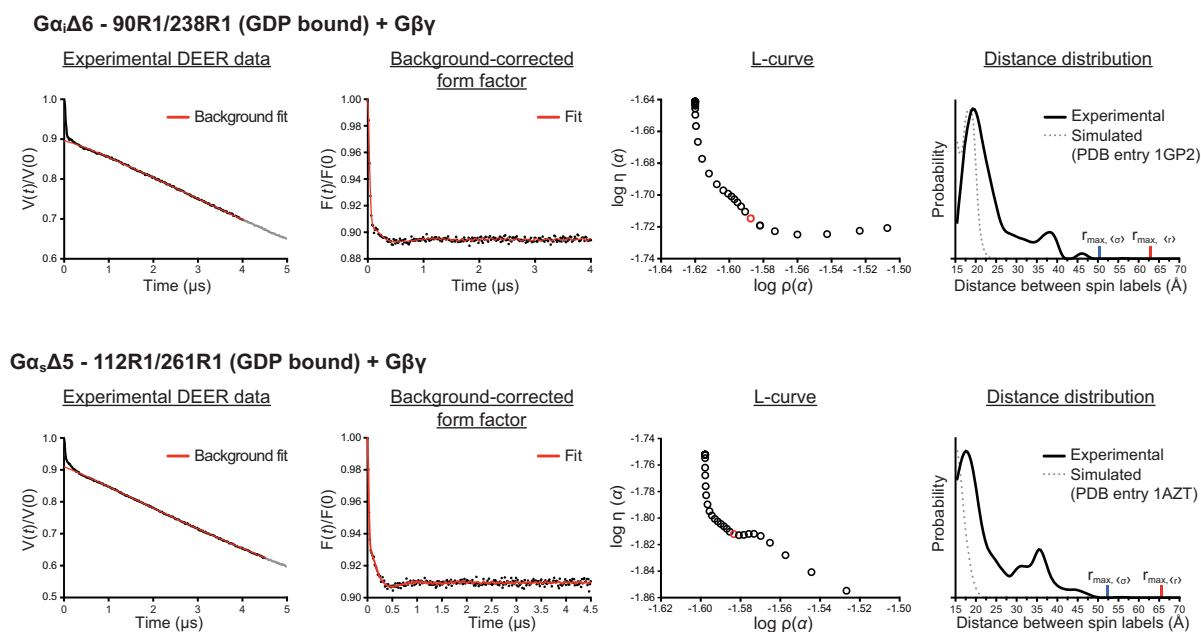
Gα_iΔ6 - 90R1/238R1 (GDP bound) + Gβγ

Gα_sΔ5 - 112R1/261R1 (GDP bound) + Gβγ

Figure S15. Q-band DEER data and analysis. Left, normalized experimental DEER data V(*t*)/V(0) (black) and background fits (red) obtained with the LongDistances software package are shown for Gα_iΔ6 R90R1/E238R1 + Gβγ and Gα_sΔ5-N112R1/N261R1 + Gβγ. Data points cut off to allow for better background fitting are shown in gray. Middle left, background-corrected normalized form factors F(*t*)/F(0) (black) and best model-free fits (red). Middle right, L-curve used for determining the optimum regularization parameter *α* (red circles). Right, experimental (black solid lines) versus simulated distance distributions (gray dotted lines). The simulated distance distributions shown here are calculated under the assumption that the G protein maintains its crystallographic GDP-bound conformation, and only the spin labels and their associated side chains move. The main peaks in the experimental distance distribution are in good agreement with the simulated interspin distances calculated using the X-ray structure of G_i bound to GDP (PDB entry 1GP2) (*5*) and Gα_i bound to GTPγS (PDB entry 1AZT) (*33*). In contrast, the peaks at longer distances are not consistent with the X-ray structures, indicating that the protein backbones must move substantially from their crystallographic conformations and suggesting that the Ras and helical domains separate spontaneously even in the GDP-bound

state. The calculated upper limits for accurate mean distances ($r_{\max,\langle r \rangle}$) and widths ($r_{\max,\langle \sigma \rangle}$) in the experimental distance distribution are shown as red and blue bars, respectively.
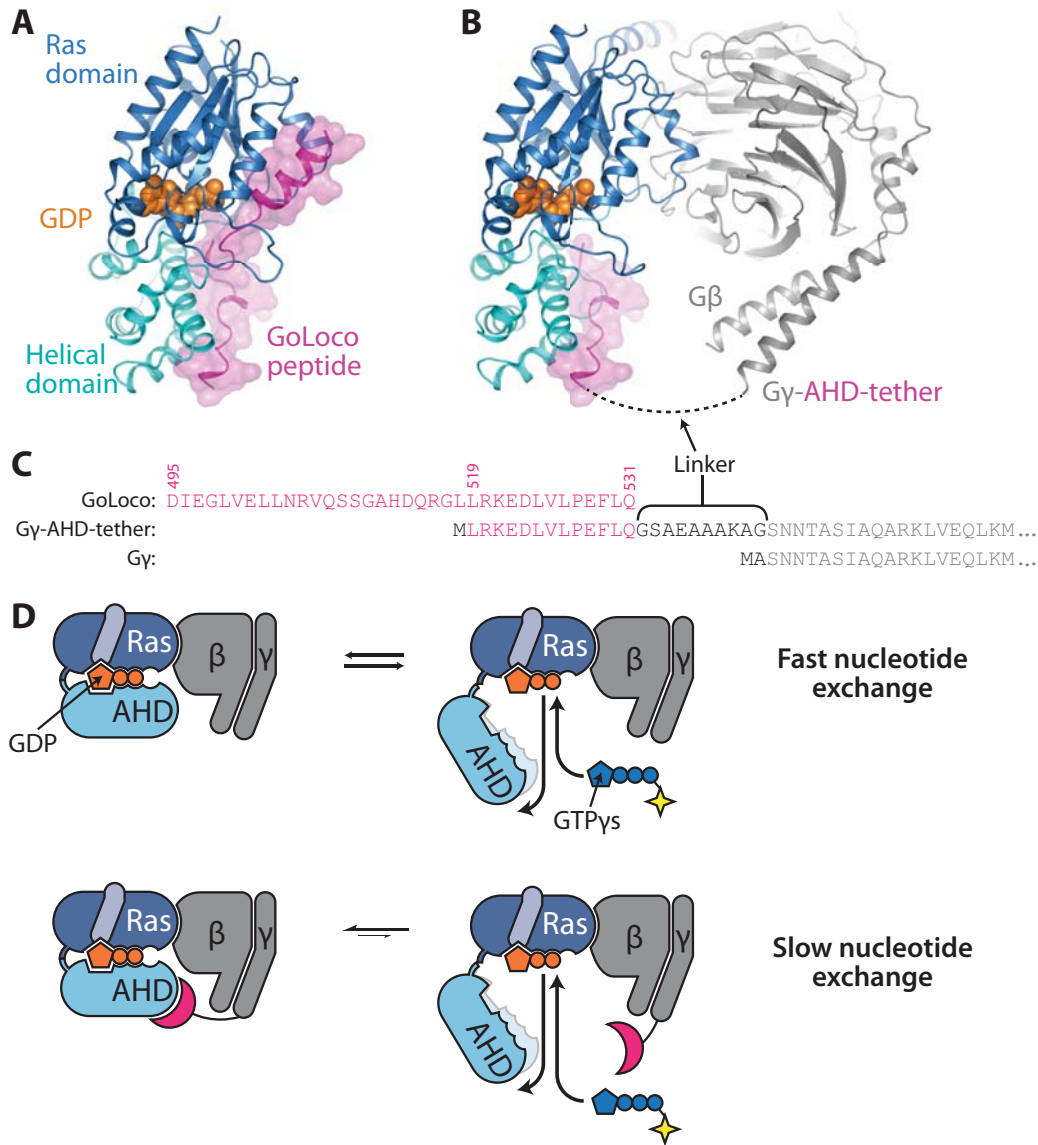
A Ras domain · GDP · Helical domain · GoLoco peptide

B Gβ · Gγ-AHD-tether · Linker

C

```
                     495                      519         531
GoLoco:        DIEGLVELLNRVQSSGAHDQRGLLRKEDLVLPEFLQ
Gγ-AHD-tether:                     MLRKEDLVLPEFLQGSAEAAAKAGSNNTASIAQARKLVEQLKM...
Gγ:                                             MASNNTASIAQARKLVEQLKM...
```

D Ras · β · γ · AHD · GDP · GTPγs · Fast nucleotide exchange · Slow nucleotide exchange

Figure S16. Gi-HD-tether construct and nucleotide-exchange kinetics assay. To test whether spontaneous domain separation plays an essential role in the nucleotide exchange process (and GDP release, in particular), we designed a G protein construct in which motion of the helical domain (HD) is restricted by a tether. We generated constructs of the G_i heterotrimer where the HD is largely constrained to be in a closed conformation by utilizing a portion of the GoLoco motif of the Regulator of G protein Signaling 14 (RGS-14). Previously crystallized co-complexes of the GoLoco peptide with $G\alpha_i$ show an extensive binding interface for the peptide

that spans both the Ras domain and the HD (A, PDB entry 3ONW) (*35*). To tether the HD in a closed conformation, a portion of the GoLoco peptide with affinity for the HD (residues 519 to 531) was fused to the amino terminus of the Gγ subunit (B). To further limit HD flexibility, we connected the GoLoco peptide fragment to Gγ using a linker sequence containing a stabilized alpha helix; some limited flexibility is afforded by Gly and Ser residues (C). Importantly, the GoLoco motif fragment that we used did not contain any of the residues that contact the nucleotide-binding site or the Ras domain in crystallized co-complexes of the GoLoco peptide with $G\alpha_i$.

(D) We assessed the role of spontaneous domain separation in nucleotide exchange by measuring the basal rate of nucleotide exchange for G_i with and without a tethered HD. Binding of the fluorescent nucleotide analog BODIPY-FL-GTPγS to G proteins de-quenches the BODIPY-FL fluorophore, yielding an increase in fluorescence that can be measured as a function of time. We observed a substantially slower association of BODIPY-FL-GTPγS to G_i with a tethered HD. Increasing the concentration of BODIPY-FL-GTPγS had minimal effect on the kinetics of nucleotide association, indicating the slower BODIPY-FL-GTPγS association kinetics primarily result from decreased GDP dissociation rate for G_i with a tethered HD. These results confirm that spontaneous domain separation is important for GDP dissociation. Nucleotide exchange does still occur (albeit very slowly) in the tethered construct, most likely reflecting the fact that the tether occasionally dissociates from the HD.
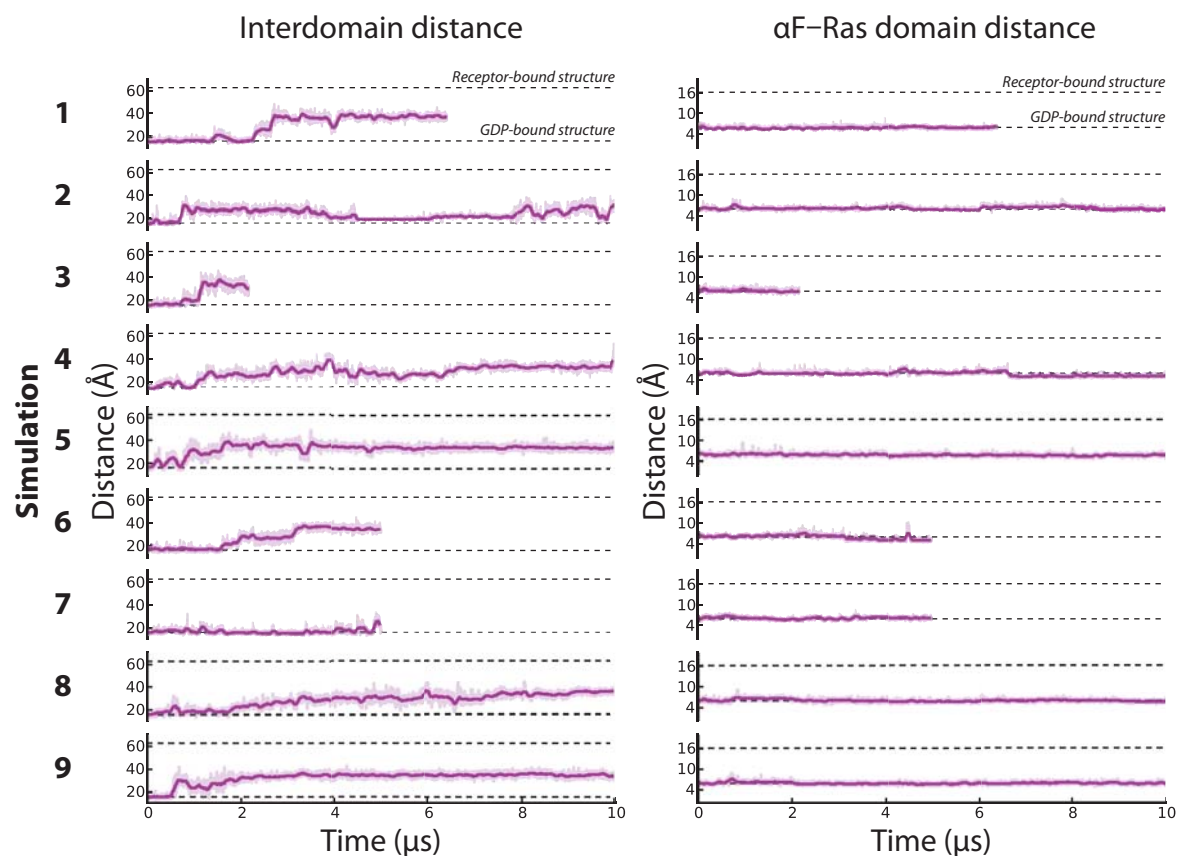
Figure S17. GDP-bound G_t simulations with and without a membrane, or with and without crystallographically unresolved residues, display similar behavior. In simulations 1–3, the membrane and lipid modifications were included, whereas in simulations 4–9, they were not. In simulations 1–6, G_t was modeled fully, whereas in simulations 7–9, the resolved crystal structure (PDB entry 1GOT) was simulated without building in missing residues. Interdomain distance and αF–Ras domain distance are measured as in Fig. 1. See *Initial coordinates and system setup* for details.

References

1. D. E. Shaw *et al.*, Millisecond-scale molecular dynamics simulation on Anton. In *Proceedings of the ACM/IEEE Conference on Supercomputing (SC09)* (ACM Press, New York, 2009).

2. D. E. Shaw *et al.*, Atomic-level characterization of the structural dynamics of proteins. *Science* **330**, 341–346 (2010).

3. S. R. Sprang, G protein mechanisms: Insights from structural analysis. *Ann. Rev. Biochem*. **66**, 639–678 (1997).

4. D. G. Lambright *et al.*, The 2.0 Å crystal structure of a heterotrimeric G protein. *Nature* **379**, 311–319 (1996).

5. M. A. Wall *et al.*, The structure of the G protein heterotrimer $G_{i\alpha1}\beta_1\gamma_2$. *Cell* **83**, 1047–1058 (1995).

6. N. P. Skiba, B. Hyunsu, H. E. Hamm, Mapping of effector binding sites of transducin α-subunit using $G\alpha_t/G\alpha_{i1}$ chimeras. *J. Biol. Chem.* **271**, 413–424 (1996).

7. S. G. F. Rasmussen *et al.*, Crystal structure of the β_2 adrenergic receptor–Gs protein complex. *Nature* **477**, 549–555 (2011).

8. K. C. Slep *et al.*, Structural determinants for regulation of phosphodiesterase by a G protein at 2.0 Å. *Nature* **409**, 1071–1077 (2001).

9. J. P. Noel, H. E. Hamm, P. B. Sigler, The 2.2 Å crystal structure of transducin-α complex with GTPγS. *Nature* **366**, 654–663 (1993).

10. A. D. MacKerell *et al.*, All-atom empirical potential for molecular modeling and dynamics studies of proteins. *J. Phys. Chem. B* **102**, 3586–3616 (1998).

11. A. D. MacKerell, M. Feig, C. L. Brooks, III, Extending the treatment of backbone energetics in protein force fields: Limitations of gas-phase quantum mechanics in reproducing protein conformational distributions in molecular dynamics simulations. *J. Comput. Chem.* **25**, 1400–1415 (2004).

12. S. Piana, K. Lindorff-Larsen, D. E. Shaw, How robust are protein folding simulations with respect to force field parameterization? *Biophys. J.* **100**, L47–L49 (2011).

13. J. B. Klauda *et al.*, Update of the CHARMM all-atom additive force field for lipids: Validation on six lipid types. *J. Phys. Chem. B* **114**, 7830–7843 (2010).

14. D. M. Rosenbaum *et al.*, Structure and function of an irreversible agonist–β_2 adrenoceptor complex. *Nature* **469**, 236–240 (2011).

15. R. O. Dror, D. H. Arlow, D. W. Borhani, M. Ø. Jensen, S. Piana, D. E. Shaw, Identification of two distinct inactive conformations of the β_2-adrenergic receptor reconciles structural and biochemical observations. *Proc. Natl. Acad. Sci. USA* **106**, 4689–4694 (2009).

16. K. Vanommeslaeghe *et al.*, CHARMM general force field: A force field for drug-like molecules compatible with the CHARMM all-atom additive biological force fields. *J. Comput. Chem.* **31**, 671–690 (2010).

17. R. O. Dror *et al.*, Activation mechanism of the β_2-adrenergic receptor. *Proc. Natl. Acad. Sci. USA* **108**, 18684–18689 (2011).

18. G. J. Martyna, D. J. Tobias, M. L. Klein, Constant pressure molecular dynamics algorithms. *J. Chem. Phys.* **101**, 4177–4189 (1994).

19. R. A. Lippert *et al.*, Accurate and efficient integration for molecular dynamics simulations at constant temperature and pressure. *J. Chem. Phys.* **139**, 164106 (2013).

20. V. Kräutler, W. F. van Gunsteren, P. H. Hünenberger, A fast SHAKE algorithm to solve distance constraint equations for small molecules in molecular dynamics simulations. *J. Comput. Chem.* **22**, 501–508 (2001).

21. M. Tuckerman, B. J. Berne, G. J. Martyna, Reversible multiple time scale molecular dynamics. *J. Chem. Phys.* **97**, 1990–2001 (1992).

22. Y. Shan, J. L. Klepeis, M. P. Eastwood, R. O. Dror, D. E. Shaw, Gaussian split Ewald: a fast Ewald mesh method for molecular simulation. *J. Chem. Phys*. **122**, 054101:1–13 (2005).

23. L. Maragliano, E. Vanden-Einjden, A temperature accelerated method for sampling free energy and determining reaction pathways in rare events simulations, *Chem. Phys. Lett.* **426**, 168–175 (2006).

24. W. Humphrey, A. Dalke, K. Schulten, VMD - Visual Molecular Dynamics. *J. Mol. Graphics* **14**, 33–38 (1996).

25. N. Van Eps *et al.*, Interaction of a G protein with an activated receptor opens the interdomain interface in the alpha subunit. *Proc. Natl. Acad. Sci. USA* **108**, 9420–9424 (2011).

26. Y. Polyhach *et al.*, High sensitivity and versatility of the DEER experiment on nitroxide radical pairs at Q-band frequencies. *Phys. Chem. Chem. Phys.* **14**, 10762–10773 (2012).

27. P. Zou, H. S. McHaourab, Increased sensitivity and extended range of distance measurements in spin-labeled membrane proteins: Q-band double electron-electron resonance and nanoscale bilayers. *Biophys. J.* **98**, L18–L20 (2010).

28. H. Ghimire, R. M. McCarrick, D. E. Budil, G. A. Lorigan, Significantly improved sensitivity of Q-band PELDOR/DEER experiments relative to X-band is observed in measuring the intercoil distance of a leucine zipper motif peptide (GCN4-LZ). *Biochemistry* **48**, 5782–5784 (2009).

29. M. Medkova, A. M. Preininger, N. J. Yu, W. L. Hubbell, H. E. Hamm, Conformational changes in the amino-terminal helix of the G protein α_{i1} following dissociation from $G\beta\gamma$ subunit and activation. *Biochemistry* **41**, 9962–9972 (2002).

30. M. T. Lerch, Z. Yang, E. K. Brooks, W. L. Hubbell, Mapping protein conformational heterogeneity under pressure with site-directed spin labeling and double electron-electron resonance. *Proc. Natl. Acad. Sci. USA* **111**, E1201–E1219 (2014).

31. G. Jeschke, DEER distance measurements on proteins. *Annu. Rev. Phys. Chem.* **63**, 419–446 (2012).

32. Y. Polyhach, E. Bordignon, G. Jeschke, Rotamer libraries of spin labelled cysteines for protein studies. *Phys. Chem. Chem. Phys.* **13**, 2356–2366 (2011).

33. R. K. Sunahara, J. J. Tesmer, A. G. Gilman, S. R. Sprang, Crystal structure of the adenylyl cyclase activator $G_{s\alpha}$. *Science* **278**, 1943–1947 (1997).

34. E. P. Marin, A. G. Krishna, T. P. Sakmar, Rapid activation of transducin by mutations distant from the nucleotide-binding site: Evidence for a mechanistic model of receptor-catalyzed nucleotide exchange by G proteins. *J. Biol. Chem.* **276**, 27400–27405 (2001).

35. D. E. Bosch *et al.*, Structural determinants of affinity enhancement between GoLoco motifs and G-protein alpha subunit mutants. *J. Biol. Chem.* **286**, 3351–3358 (2011).